LA-8757-PR

Progress Report

C.3

Applied Nuclear Data Research and Development

October 1—December 31, 1980

University of California

LOS ALAMOS SCIENTIFIC LABORATORY
Post Office Box 1663 Los Alamos, New Mexico 87545

The four most recent reports in this series, unclassified, are LA-8298-PR, LA-8418-PR, LA-8524-PR and LA-8630-PR.

This report was not edited by the Technical Information staff.

This work was performed under the auspices of the US Department of Energy's Division of Reactor Research and Technology, Office of Basic Energy Sciences, and Office of Fusion Energy; and the Electric Power Research Institute.

UNITED STATES
DEPARTMENT OF ENERGY
CONTRACT W-7405-ENG. 36

LA-8757-PR
Progress Report

UC-34c
Issued: March 1981

Applied Nuclear Data Research and Development

October 1—December 31, 1980

Compiled by

C. I. Baxman
P. G. Young

TABLE OF CONTENTS

APPLIED NUCLEAR DATA RESEARCH AND DEVELOPMENT

OCTOBER 1 - DECEMBER 31, 1980

Compiled by

C. I. Baxman and P. G. Young

ABSTRACT

This progress report describes the activities of the Los Alamos Nuclear Data Group for October 1 through December 31, 1980. The topical content is summarized in the Table of Contents.

I. THEORY AND EVALUATION OF NUCLEAR CROSS SECTIONS

A. Coulomb Corrections in the Three Nucleon System [G. M. Hale and H. Zankel (T-5)]

An interesting area of study in reactions among light nuclei is the comparison of mirror reactions (reactions related by the interchange of protons and neutrons). There has been increasing experimental activity in this area over the past five years, and in the several instances where large differences in data for mirror reactions have been observed, the inevitable question is raised, "are these differences compatible with charge-symmetric nuclear forces?" Our charge-independent R-matrix studies[1] indicate that generally they are, but these studies have used quite simple corrections for internal Coulomb effects in light nuclei. Another approach developed recently by Zankel and his collaborators[2-4] involves using an approximation to the two-potential integral equations for the transition operator[5] in order to make Coulomb corrections in light nuclei, assuming the nuclear forces are charge-symmetric. We have applied this method to nucleon-deuteron scattering, where such corrections are of great interest, since all the theoretical calculations are for n-d and most of the measurements are for p-d.

A sample of these calculations is shown in Fig. 1 for the deuteron tensor analyzing power T_{20} at E_d = 10 MeV (E_N = 5 MeV). The solid curve is calculated

from p-d phase shifts[6] that represent the measurements well at this energy. The dashed curve is calculated from the same phase shifts, omitting contributions from the Coulomb amplitude and asymptotic Coulomb phase shifts. This is the type of correction normally made to relate the n-d calculations and p-d measurements. It can be seen to give in this case a small difference, except at forward angles. The dash-dot curve is our prediction for n-d, which includes in addition to the asymptotic Coulomb effects an approximate correction for the Coulomb distortion of the "nuclear" T matrix. This calculation differs markedly from the p-d curve in the minimum at θ_{cm} = 105 degrees and corresponds more closely to the differences seen in n-d calculations and p-d measurements. Of course, it would be highly desirable to have n-d measurements for T_{20}, but this difficult experiment has not yet been done.

Our calculations indicate that this approximate Coulomb correction is an improvement over the simple one normally used. It can be used to correct n-d calculations for comparisons with p-d data (or vice versa) and to guide experimentalists in judging what sort of differences between p-d and n-d measurements are consistent with charge-symmetric nuclear forces.

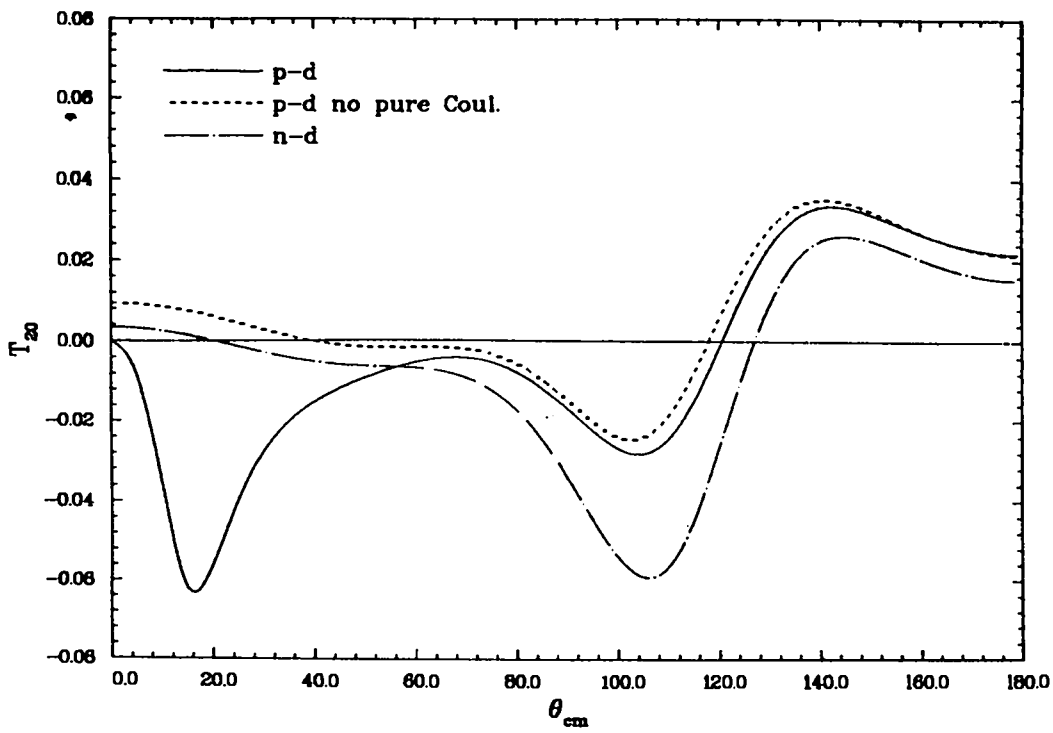

Fig. 1.
Calculations of the tensor analyzing power T_{20} for deuteron-nucleon scattering at 10 MeV.

B. Gamma-Ray Production Cross Section Calculations for the Tungsten Evaluation (E. D. Arthur)

One reason for the use of extensive nuclear model calculations for our new tungsten evaluation (see following contribution) was to ensure a consistency between evaluated neutron and gamma-ray files, a situation that does not exist for the present ENDF/B-V tungsten evaluation. Comparison of our calculated gamma-ray production spectra to measurements made by Dickens et al.[7] showed some disagreement, particularly for incident neutron energies between 6 and 10 MeV. An example of this disagreement is shown in Fig. 2 for the gamma-ray spectrum induced by 6.25-MeV neutrons on natural tungsten. Since experimental measurements of low-energy gamma rays can be difficult because of electronic threshold and spectrum unfolding effects, the disagreement below 1 MeV was not considered serious. However, the disagreement in the secondary gamma-ray energy region between 2.5 and 5.5 MeV was more worrisome since in our calculations the majority of these gamma rays occur because of inelastic scattering. Attempts to adjust input to the calculations in a reasonable manner produced little change (<20%) in the calculated spectrum. Even unphysical manipulations of level density, optical model, and gamma-ray strength function parameters failed to provide agreement with this data.

To further test our theoretical results, we calculated gamma-ray production spectra for 6.5-MeV neutrons on ^{181}Ta, the nearest neighbor for which such measurements[8] were available. Parameters similar to those determined for ^{182}W calculations were used. The results are shown in Fig. 3 where good agreement occurs in the secondary gamma-ray energy range between 2.5 and 5.5 MeV. The main cause of the differences between the ^{181}Ta and tungsten calculated spectra appear to be related to the level densities of the target nuclei. For the tungsten calculation most of the contribution arises from neutron interactions with even-even isotopes whose level density is substantially lower than that for the odd-odd ^{181}Ta nucleus. Figure 4 illustrates the difference between the number of levels available for inelastic scattering from ^{181}Ta and from the even-even tungsten isotope, ^{182}W.

Our tungsten calculations were further corroborated by other data measured in this energy region by Drake[9] and by Savin.[10] Figure 5 compares our calculated spectrum to these data. Thus, because of the difficulties in reproducing the ORNL data through nuclear-model calculations, the theoretical level-density arguments that appear to support our calculations, and the data that agree with

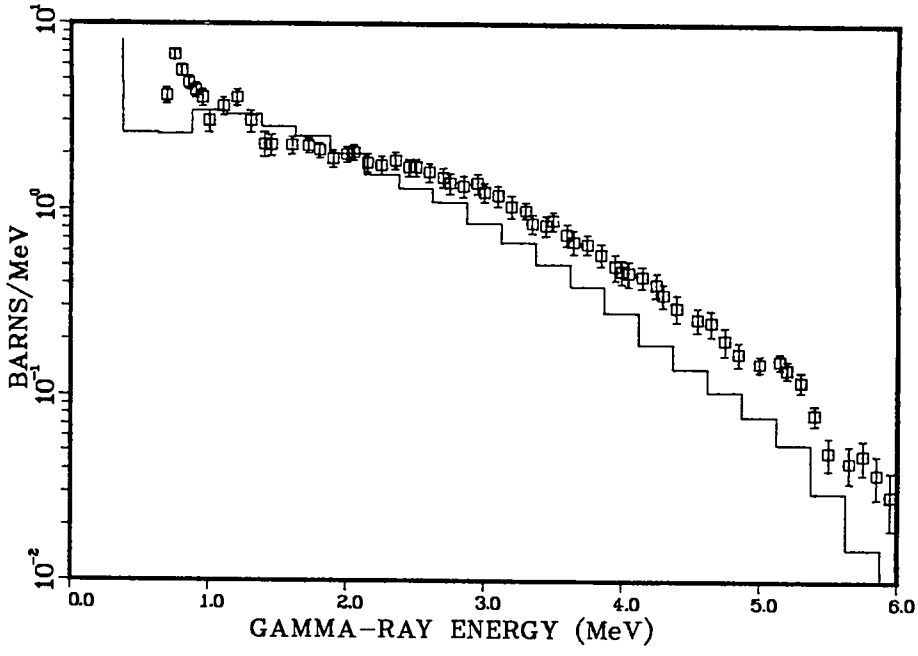

Fig. 2.
The calculated tungsten gamma-ray production spectrum induced by 6.25 MeV neutrons is compared to the data of Dickens.[7]

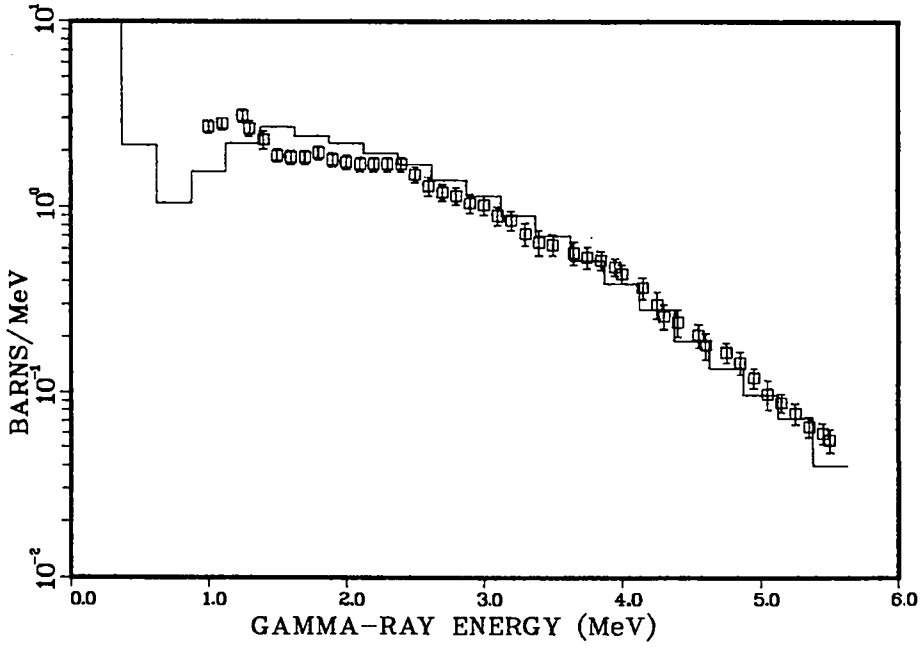

Fig. 3.
Calculated and measured[8] gamma-ray production spectra induced by 6.5 MeV neutrons on ^{181}Ta.

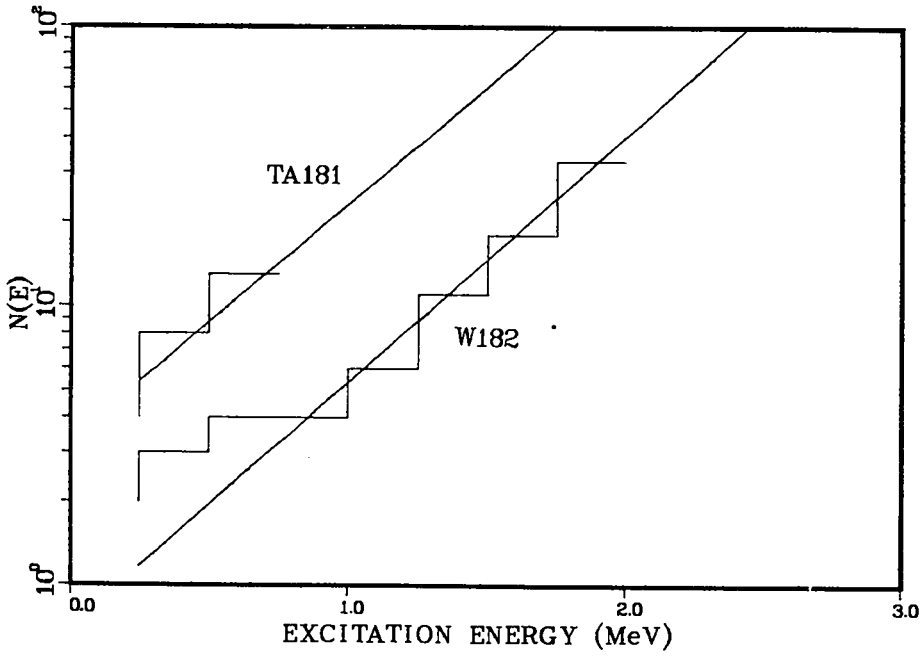

Fig. 4.
A comparison of the cumulative number of levels for the even-even ^{182}W nucleus and the odd-odd ^{181}Ta nucleus.

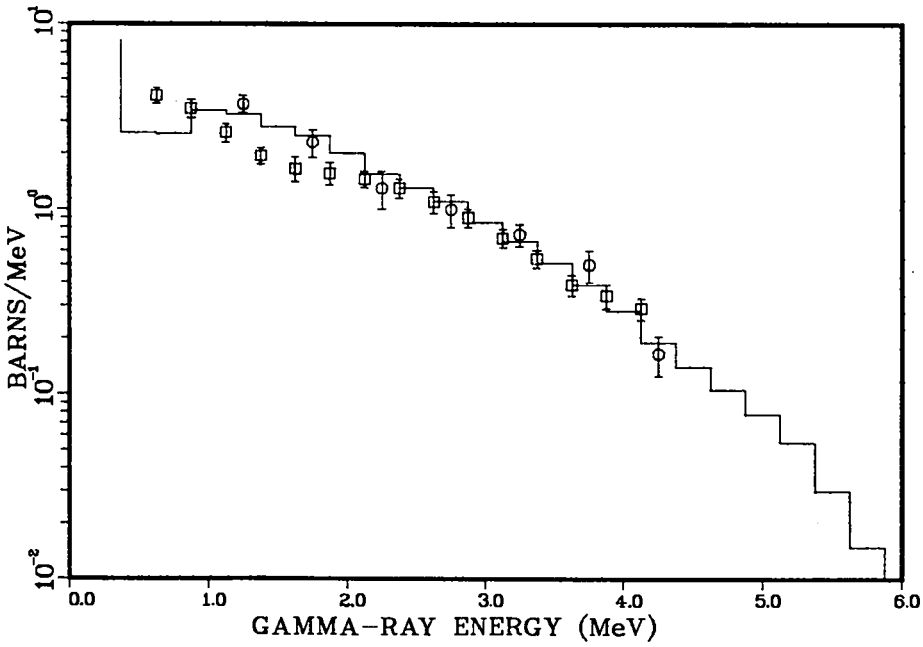

Fig. 5.
Our calculated gamma-ray production spectrum for 6.25-MeV neutrons on tungsten is compared to the Drake[9] (squares) and Savin[10] (circles) measurements.

our results, we have decided to use our calcuated gamma-ray production spectra thoughout the entire evaluation, even though in some cases they do not agree with the Oak Ridge measurements. Further experimental measurements are clearly needed to resolve this discrepancy.

C. $^{182,183,184,186}W$ Evaluations [E. D. Arthur, P. G. Young, A. B. Smith (ANL), and C. A. Philis (Bruyeres-le-Chatel)]

New evaluations for the tungsten isotopes have been completed in the energy range from 0.1 to 20 MeV. These results were combined with ENDF/B-V data below 0.1 MeV to produce evaluated data files applicable over the energy range from 10^{-5} eV to 20 MeV. These new evaluations incorporate recently measured experimental results and correct many of the deficiencies of the previous ENDF/B evaluations, particularly with regard to energy balance and the spectra of emitted neutrons.

Our previous progress report[11] presented background on the techniques and philosphy used in this evaluation. In summary, nuclear models that describe neutron reactions in this mass and energy range--coupled-channel deformed optical model, Hauser-Feshbach statistical, and preequilibrium--were optimized to experimental data and used to produce most of the desired cross sections and spectra. Parameter sets (neutron optical, gamma-ray strength functions, level density) were employed that reproduce, in a consistent manner, differing reaction data available for these nuclei in the energy range listed above. By the use of calculated results to produce the evaluated data, consistency is maintained between neutron and gamma-ray files. In addition, a reliable method is provided whereby evaluated data can be obtained in mass and energy regions lacking experimental measurements.

Table I lists the reactions, their thresholds, and MT numbers appearing in the present evaluation. Evaluated total cross sections were obtained for the even-even tungsten isotopes through use of experimental data, particularly recent measurements[12] made in the energy region from 0.2 to 5 MeV as well as guidance from deformed optical-model calculations. Figure 6 compares the evaluated total cross sections for ^{182}W to available data. The evaluated total cross section below 1 MeV is based on the new Argonne results of Ref. 12. For ^{182}W, these new measurements are consistent with previous measurements by Martin.[13] However, for ^{184}W and ^{186}W the new Argonne data do not agree with the Martin data so that the evaluated total cross section differs substantially from the

ENDF/B-V values below 2 MeV. Since no experimental total cross sections exist above 15 MeV, theoretical results from coupled-channel calculations were used between 15 and 20 MeV. Similarly, because of the complete absence of experimental data, evaluated total cross sections for ^{183}W are based exclusively on such calculated results between 0.1 and 20 MeV.

For inelastic scattering to discrete levels we used only those levels whose properties (excitation energy, spin, parity) have been fully identified. These levels and their MT numbers also appear in Table I. At excitation energies where knowledge of such discrete levels becomes sparse or fragmented, we used a continuum representation rather than employing fictitious levels. By doing so, we preserved a continuity in the calculated results over the entire incident energy range. Note that the continuum cross section denoted by MT=91 in Table I generally has a threshold lying much lower than those of the uppermost discrete level. In these cases MT=91 includes contributions from the (n,γn') process that has non-negligible cross-section values, at least until incident energies where the continuum (n,n') process dominates.

Figures 7 through 9 compare the evaluation to selected experimental results for reaction types that dominate within the 1 to 20 MeV energy range. Since the evaluated results were obtained from nuclear-model calculations, such comparisons illustrate how well such techniques can reproduce varied data in a consistent manner. The evaluated elastic for ^{184}W and the inelastic cross sections to the 2^+ and 4^+ rotational states in ^{186}W appear in Figs. 7 and 8. In these instances, both Hauser-Feshbach and coupled-channel direct-reaction models govern the calculated results. Finally, Fig. 9 presents a comparison of the evaluated $^{183}W(n,2n)$ cross section to data[14] measured from threshold to 15 MeV. Similar agreement was obtained for (n,2n) cross sections on the even-even tungsten isotopes (see Ref. 11).

TABLE I

REACTIONS AND THEIR THRESHOLDS FOR THE $^{182,183,184,186}W$ EVALUATIONS

^{182}W

MT	E_{th}(MeV)	Reaction Description	
1	EXO	Total	
2	EXO	Elastic	
3	EXO	Nonelastic	
4	0.1006	Total Inelastic	
16	8.1071	(n,2n)	
17	14.829	(n,3n)	
28	7.1313	(n,np)	
		(n,n')	to ^{182}W state
51	0.1006		0.1005 MeV
52	0.3080		0.32898
53	0.6838		0.68003
54	1.1420		1.1357
55	1.1508		1.1445
56	1.2290		1.2222
57	1.2650		1.258
58	1.296		1.2889
59	1.338		1.3306
60	1.378		1.3704
61	1.448		1.44
62	1.495		1.4868
63	1.5180		1.5096
64	1.562		1.5534
65	1.631		1.622
66	1.642		1.6329
67	1.67		1.6608
68	1.721		1.7115
69	1.768		1.7583
91	0.3	Continuum Inelastic --(n,γn') and (n,n')	
102	EXO	Capture	
103	1.0343	(n,p)	
107	EXO	(n,α)	

^{183}W

MT	E_{th}(MeV)	Reaction Description	
1	EXO	Total	
2	EXO	Elastic	
3	EXO	Nonelastic	
4	0.04726	Total Inelastic	
16	6.2246	(n,2n)	
17	14.331	(n,3n)	
28	7.2588	(n,np)	
		(n,n')	to ^{183}W state
51	0.04726		0.047 MeV
52	0.09955		0.099
53	0.2081		0.20696
54	0.2102		0.20905
55	0.2936		0.29199
56	0.3107		0.309
57	0.3112		0.3095
58	0.4143		0.4120
59	0.4555		0.453
60	0.4897		0.487
61	0.5571		0.5541
62	0.6033		0.5999
63	0.6234		0.6199
64	0.7441		0.74
91	0.7441	Continuum Inelastic	
102	EXO	Capture	
103	2.876	(n,p)	
107	EXO	(n,α)	

TABLE I (cont.)

^{184}W

MT	E_{th}(MeV)	Reaction Description
1	EXO	Total
2	EXO	Elastic
3	EXO	Nonelastic
4	0.118	Total Inelastic
16	7.4511	(n,2n)
17	13.676	(n,3n)
28	7.74	(n,np)
		(n,n') to ^{184}W state
51	0.118	0.1119 MeV
52	0.3	0.29836
53	0.7524	0.7483
54	0.9082	1.9033
55	1.008	1.0025
56	1.012	1.0065
57	1.1280	1.1219
58	1.136	1.1299
59	1.14	1.1338
60	1.228	1.2214
61	1.292	1.285
62	1.301	1.294
63	1.329	1.3218
64	1.352	1.3447
65	1.366	1.3586
66	1.394	1.3865
67	1.433	1.4253
68	1.439	1.4312
91	0.5	Continuum Inelastic --(n,γn') and (n,n')
102	EXO	Capture
103	2.0953	(n,p)
107	EXO	(n,α)

^{186}W

MT	E_{th}(MeV)	Reaction Description
1	EXO	Total
2	EXO	Elastic
3	EXO	Nonelastic
4	0.123	Total Inelastic
16	7.2386	(n,2n)
17	13.024	(n,3n)
28	8.4727	(n,np)
		(n,n') to ^{186}W state
51	0.123	0.1223 MeV
52	0.3987	0.39655
53	0.7415	0.7375
54	0.8129	0.8086
55	0.8665	0.8619
56	0.8680	0.8821
57	0.9576	0.9525
58	1.011	1.0056
59	1.021	1.0155
60	1.037	1.0315
61	1.051	0.0454
62	1.156	1.1498
63	1.286	1.2791
64	1.291	1.2841
65	1.305	1.298
66	1.326	1.3189
67	1.471	1.4631
68	1.528	1.5198
91	0.3	Continuum Inelastic --(n,γn') and (n,n')
102	EXO	Capture
103	3.1325	(n,p)
107	EXO	(n,α)

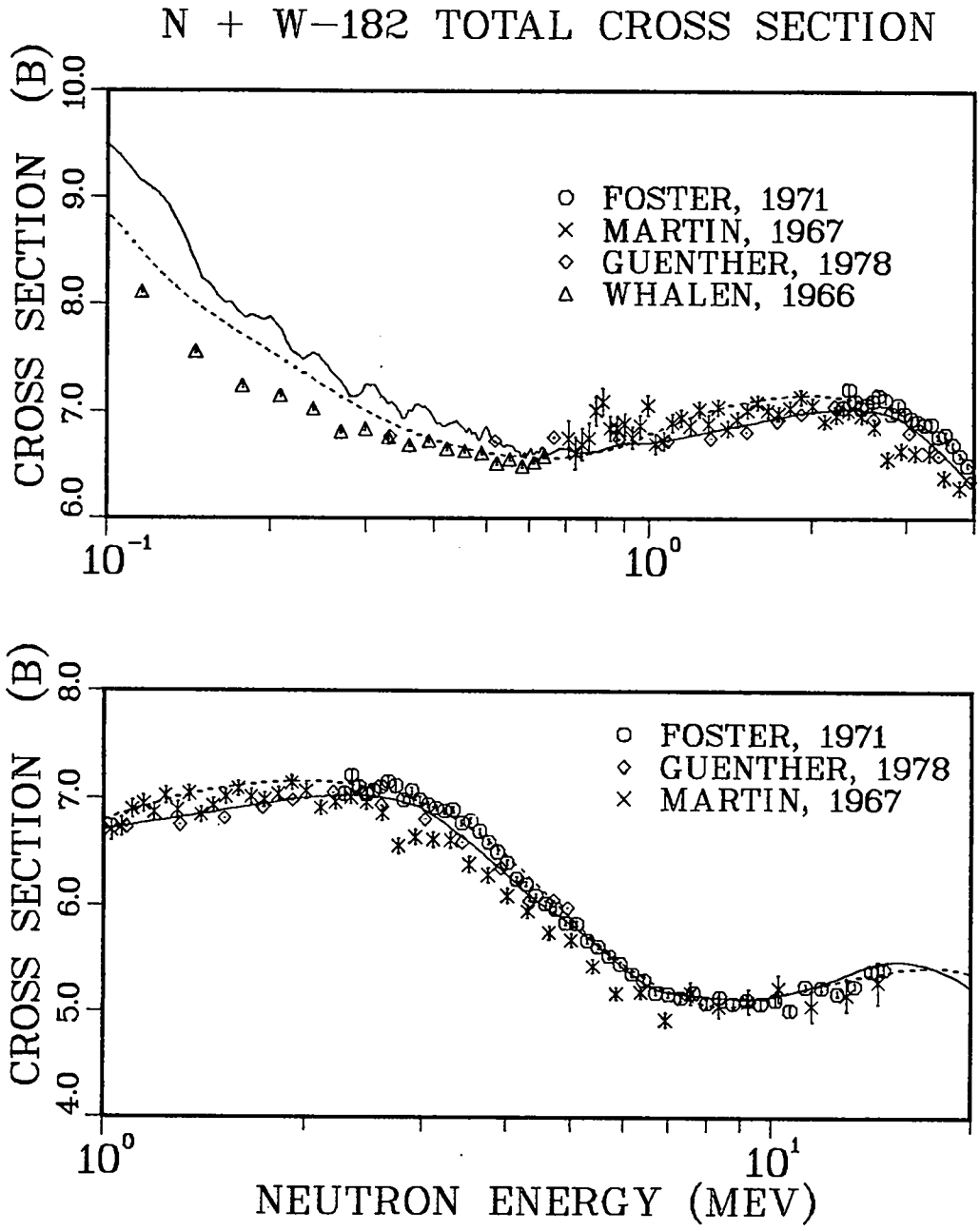

Fig. 6.
Evaluated (solid curve) and experimental values for the ^{182}W total cross section. The dashed curve is ENDF/B-V.

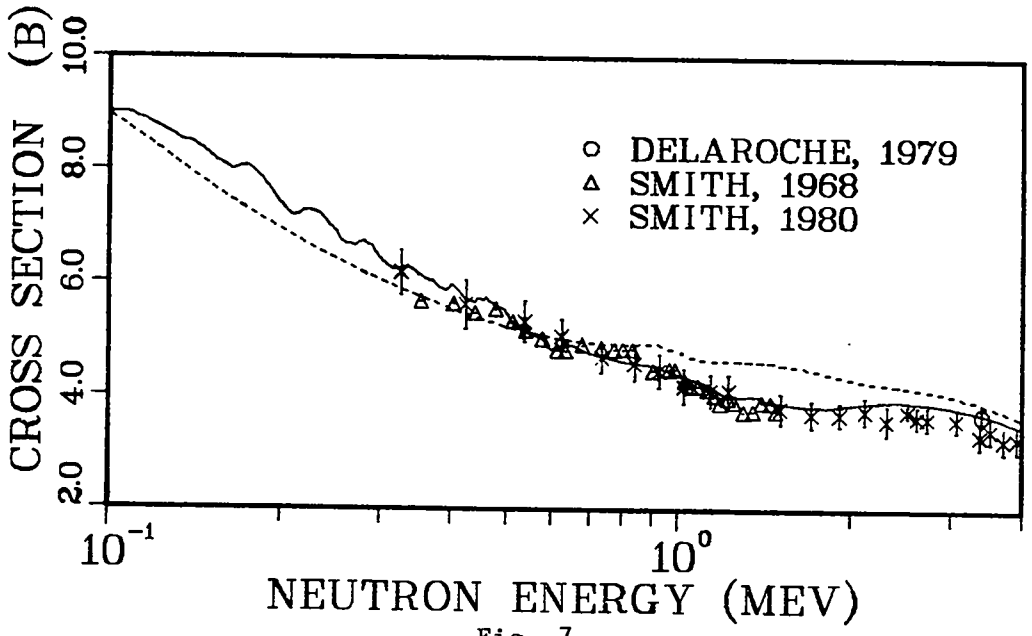

Fig. 7.
The evaluated elastic cross section is compared to experimental data available for ^{184}W. ENDF/B-V is the dashed line.

D. Average Neutronic Properties of "Prompt" Fission Products (D. G. Foster, Jr., and E. D. Arthur)

The goal of this program is to calculate complete average neutronic properties of the ensemble of fission products from fast fission of ^{235}U and ^{239}Pu, where the average is computed before the first beta decay has occurred. We have now finished these calculations, which cover the range in incident neutron energy in the laboratory system from 0.001 to 20 MeV. They include the (n,γ), elastic-scattering, inelastic-scattering, (n,2n), and (n,3n) reactions. For each reaction, we have calculated the cross sections and spectra of neutrons and photons and the angular distributions of the neutrons. The integrated cross sections are shown in Figs. 10 and 11, for fission products from ^{235}U and ^{239}Pu, respectively. The results are in ENDF/B format.

In Ref. 15 we discussed the selection of nuclides to be used in a weighted average to approximate the ensemble of many hundreds of fission-product nuclides. We also described how we derived the nuclear-model parameters for the 44 nuclides needed in the calculations. Subsequently, we were forced to change the state-density constant used in the preequilibrium model[16] incorporated into GNASH. The standard value, A/13 (A is the mass number of the target nuclide) gives unrealistically large low-energy preequilibrium fractions for $^{87,88}Se$, $^{92,93}Kr$, and ^{95}Sr. Accordingly, for all isotopes of Se, Kr, and Sr we arbitrarily increased this constant by approximately 30%, which is sufficient to keep

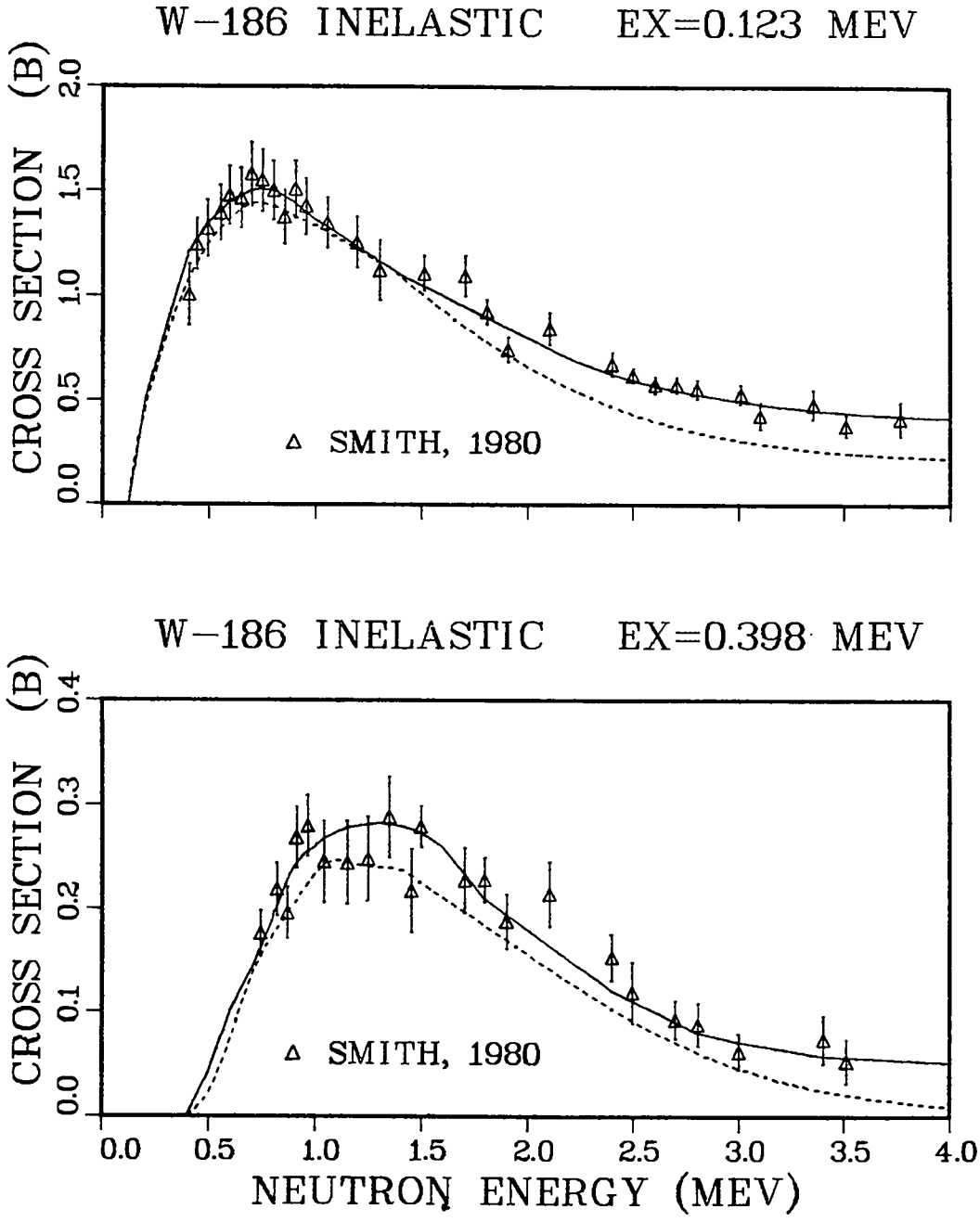

Fig. 8.
A comparison of the evaluated and experimental cross sections for neutron inelastic scattering from the 2^+ and 4^+ rotational states in ^{186}W. (Dashed lines are ENDF/B-V.)

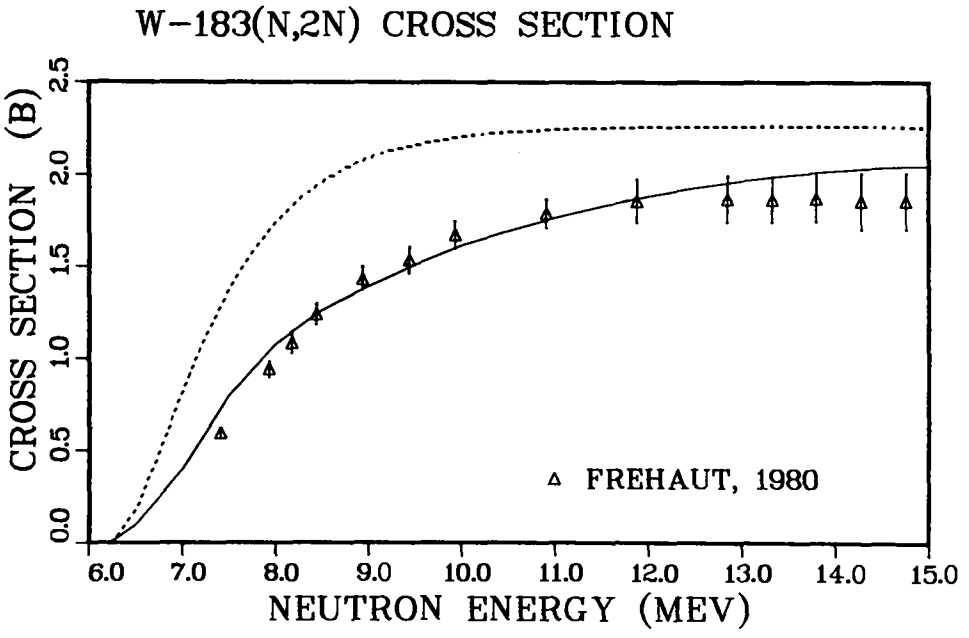

Fig. 9.
The evaluated (n,2n) cross sections for ^{183}W is compared to the Frehaut[4] measurements from threshold to 15 MeV. The dashed curve is ENDF/B-V.

the preequilibrium fractions below 0.3 at 10 MeV. In addition, in order to improve the treatment of low-energy inelastic scattering, we deduced plausible energies, spins, and parities from nuclear systematics for the first excited states of 9 of the 19 targets used in these calculations.

Figure 12 summarizes the calculations carried out for each of the target nuclides. COMNUC,[17] which is best suited to low incident energies, supplies cross sections from 0.001 to 5 MeV. It also supplies angular distributons for elastic and inelastic scattering to discrete final states. GNASH,[16] which is best suited to higher neutron energies, supplies cross sections between 1 and 20 MeV, with neutron and photon spectra but no angular distributions. Cross sections calculated by the two codes agree well near 5 MeV. The 4-MeV overlap region permits generating smooth angular distributions and spectra by combining the results of the two codes.

COMNUC is entirely self-contained and consequently takes all of its input information from cards. GNASH, on the other hand, is the key element in a family of codes and postprocessors and takes only the case description from cards. It uses external files of transmission coefficients (calculated by TCCAL[18]), level properties, and ground-state mass excesses. We use it in its basic mode

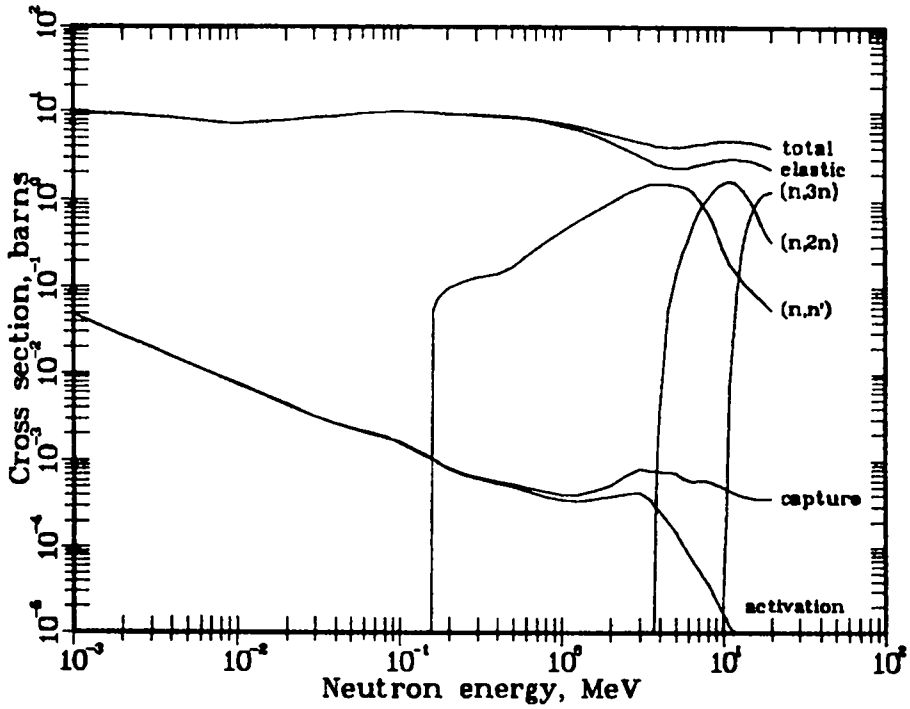

Fig. 10.
Calculated neutron cross sections of an "average prompt fission product" from the fission of ^{235}U by fast neutrons.

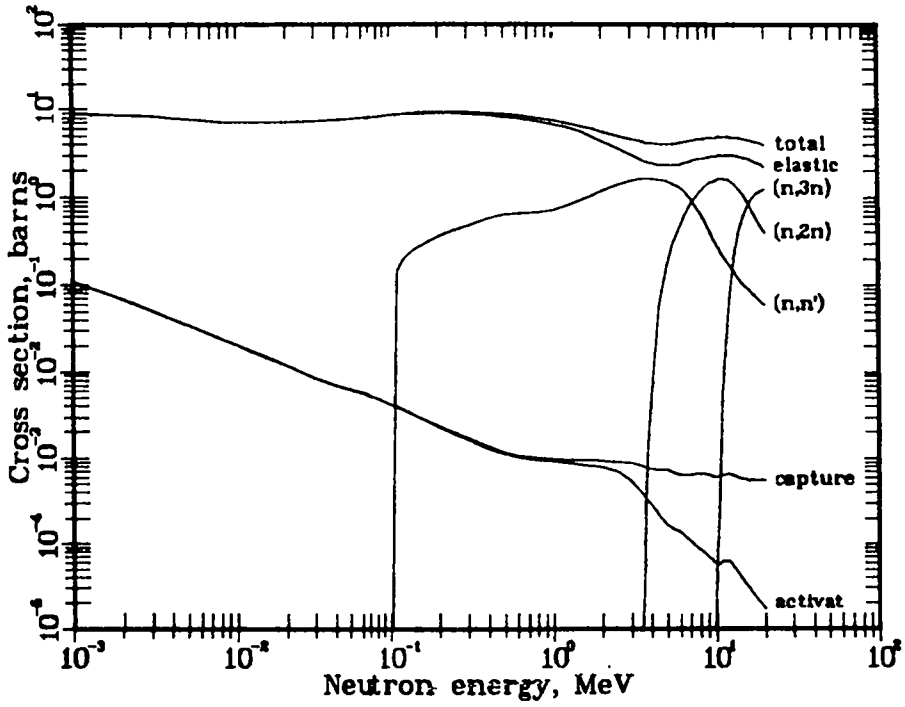

Fig. 11.
Calculated neutron cross sections of an "average prompt fission product" from the fission of ^{239}Pu by fast neutrons.

to generate output files of cross sections and bin populations that can be used to construct spectra of neutrons and photons from the (n,n'), (n,2n), and (n,3n) reactions. Since it deals only with the non-elastic part of the initial interaction, we use SCAT[19] to supply the shape-elastic cross section and angular distribution. Operating in an alternate mode, GNASH writes an additional file containing the complete photon spectrum from the (n,γ) and (n,γn) processes in the initial compound nucleus, along with the resulting cross section for reaching the ground state of the nuclide of mass A+1, which is the activation cross section shown in Figs. 10 and 11. Although GNASH does not calculate secondary neutron angular distributions explicitly, it does calculate the preequilibrium fraction, which can be combined with the secondary-neutron energy to generate coupled energy-angular distributions using the systematics of Kalbach and Mann.[20]

It is evident from Fig. 12 that GNASHRD serves to gather the separate fragments from the GNASH "family" into a single set of cross sections, spectra, and angular distributions. Subsequently, CONSOL joins the GNASH results to the low-energy data from COMNUC and constructs a smooth transition between the two data sets.

The final steps in these calculations are not shown in Fig. 12. A simple code called AVERAGE reads ten input files generated by CONSOL and prepares a composite weighted average that approximates the neutronic properties of the ensemble of fission products. The nuclides and their weights were determined separately, from the yield curves for fission of ^{235}U and ^{239}Pu, as outlined in

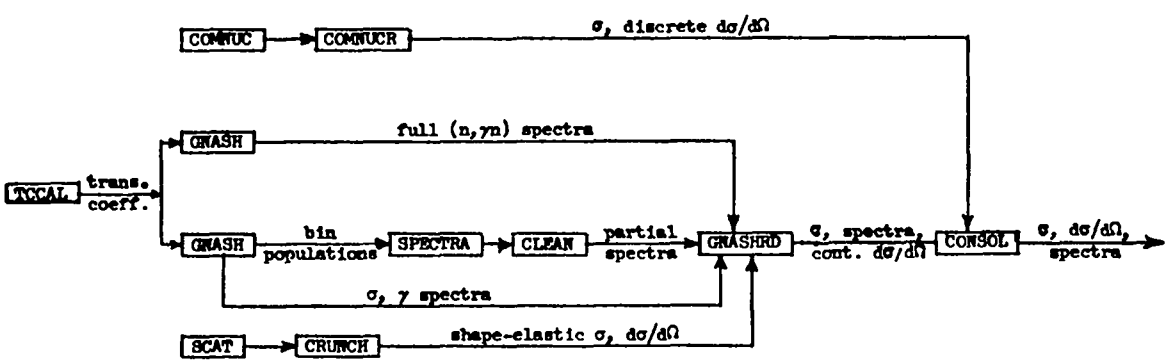

Fig. 12.
Flow chart of calculations.

Ref. 15 (^{138}Xe is the only nuclide common to both sets). A final code SIGMA generates the appropriate shape for the cross-section curves near the (n,n'), (n,2n), and (n,3n) thresholds and generates cross sections on a finer mesh using spline interpolation. SIGMA then generates the ENDF/B representation of the composite data set and prepares tabulations and plots.

The coupled-energy angle distributions that emerge from AVERAGE should logically go into File 6 of ENDF/B, but the existing formats are inappropriate for distributions derived from the Kalbach-Mann formalism, which take the form of attaching angular distributions to each bin of a secondary energy histogram. The results of our calculations are being prepared in more than one form, including the use of proposed new formats[21] for File 6 that are better suited to the Kalbach-Mann approach.

A more detailed description of these calculations will be issued as a Los Alamos National Laboratory report in the near future.

E. Calculation of Prompt Fission Neutron Spectra for ^{242}Pu(sf) and ^{252}Cf(sf) (D. G. Madland)

The prompt fission neutron spectrum N(E) has been calculated for the spontaneous fission of ^{242}Pu and ^{252}Cf. The calculations have been performed for emitted neutron energies E ranging from 0.1 keV to 20.0 MeV. The physical units used are E (MeV) and N(E) (MeV^{-1}). The theoretical spectrum is defined such that

$$\int_0^\infty N(E)dE = 1 \quad .$$

The theoretical work upon which these calculations are based in described in Refs. 22 and 23 and in a report now being prepared. The present calculations were performed using the "Simulated Energy-Dependence of $\sigma_c(\varepsilon)$" approach, which is discussed in the report being prepared. While little or no experimental prompt fission neutron spectra data exist for ^{242}Pu(sf), they do exist for ^{252}Cf(sf) and are in good agreement with our calculation. Experimental data also exist for the average prompt neutron multiplicity $\bar{\nu}_p$ for these cases. Since the formalism that we use to calculate N(E) is also used to calculate $\bar{\nu}_p$, a test of the N(E) calculation is made by comparing calculated and measured $\bar{\nu}_p$ values. For the present calculation, the results are

$^{242}Pu(sf)$: $\bar{\nu}_p$ (exp) = 2.141 ± .009

$\bar{\nu}_p$ (calc) = 2.151

Relative Difference = 0.47% ,

$^{252}Cf(sf)$: $\bar{\nu}_p$ (exp) = 3.757 ± .009

$\bar{\nu}_p$ (calc) = 3.788

Relative Difference = 0.83% ,

where the experimental data are from Refs. 24 and 25. Because the $\bar{\nu}_p$ calculation relies heavily upon energy balance in the fission process, the excellent agreement between experiment and theory indicates that the correct energy dissipation was used in calculating N(E). This, in turn, means that the slope of the tail of N(E) is correctly calculated.

F. Calculation of Watt Distribution Parameters for Spontaneous and Neutron-Induced Fission (D. G. Madland)

Prompt fission neutron spectra for both spontaneous and neutron-induced fission were calculated in the Watt distribution approximation. These calculations were performed using the parameters of a "Simulated energy-dependence of $\sigma_c(\varepsilon)$" approach, which itself is an approximation to a more exact calculation, both of which are discussed in a report now being written. The present results are given in Table II in terms of constants C_1, C_2, and C_3, which are related to the Watt distribution parameters A_{Watt} and B_{Watt} by

$$A_{Watt}(E_n) = \frac{8}{9}\left[\frac{C_1 + E_n\ (\text{MeV}}{C_2}\right]^{1/2} \quad \text{MeV},$$

$$B_{Watt}(E_n) = \frac{81}{16}\left[\frac{C_3}{C_1 + E_n\ (\text{MeV})}\right] \quad \text{MeV}^{-1},$$

where E_n is the kinetic energy of the neutron inducing fission. The energy E_n is not to exceed the threshold for second-chance fission. Thus, the Watt parameters of Table II are valid for $0 \leq E_n \leq \approx$ 5-7 MeV. Note that E_n is set to zero in the case of spontaneous fission. The definitions of A_{Watt} and B_{Watt} are found in Ref. 26.

TABLE II

CONSTANTS FOR THE CALCULATION OF THE WATT DISTRIBUTION APPROXIMATION TO THE PROMPT FISSION NEUTRON SPECTRUM FOR SEVERAL FISSIONING SYSTEMS

Fission Reaction	C_1	C_2	C_3
$^{233}U + n(E_n)$	23.716	23.4	18.472
$^{235}U + n(E_n)$	21.726	23.6	18.417
$^{238}U + n(E_n)$	21.172	23.9	18.145
$^{239}U + n(E_n)$	21.196	24.0	18.163
$^{240}U + n(E_n)$	19.842	24.1	18.182
$^{239}Pu + n(E_n)$	25.921	24.0	18.775
$^{240}Pu(sf)$	19.387	24.0	18.775
$^{240}Pu + n(E_n)$	26.890	24.1	18.708
$^{242}Pu + n(E_n)$	28.598	24.3	18.541
$^{242}Cm(sf)$	24.338	24.2	19.453
$^{244}Cm(sf)$	25.375	24.4	19.285
$^{252}Cf(sf)$	33.508	25.2	19.365

II. NUCLEAR CROSS SECTION PROCESSING

A. Code Development (R. B. Kidman)

Over the years several improvements to 1DX have been investigated. A new code, SUPERX, has been started, which is an overhaul of 1DX incorporating those improvements. To date SUPERX contains the following changes.

1. Improved f-factor interpolation,
2. Improved elastic downscatter iteration,
3. Elastic scattering matrices,
4. Elastic downscatter f-factors,
5. A new transport cross-section computation, and
6. Isotope and region-dependent source matrices.

Future plans include the following additions to SUPERX.

1. Leakage correction to the background cross section,
2. An improved diffusion coefficient computation,
3. Spectral adjustments to all cross sections, and
4. Higher order transfer cross sections.

The development of SUPERX requires changes to other codes in the chain. CINX has been modified to pass along elastic removal factors, elastic scattering matrices, and isotope chi matricies. SUPERB is an overhaul of PERTV and can now use isotope and region-dependent fission chi matrices.

B. Benchmark Testing (R. B. Kidman)

The 93-isotope, 70-group library (LIB-V) generated last quarter from the latest ENDF/B-V data was used with SUPERX and SUPERB to compute parameters for 17 fast benchmark criticals. The uncorrected, diffusion theory eigenvalues are shown in Table III and compared to the old 1DX values. Much larger changes occur in reaction rate ratios, worths, and spectra. A complete set of our current results has been sent to the Cross Section Evaluation Working Group (CSEWG).

C. Data Processing (R. B. Kidman)

The latest LIB-V library has been sent to Hanford, Westinghouse, and General Electric. Normally, at Los Alamos we generate and use LIB-V as a binary file so we are never concerned with round-off error. However, when we send out LIB-V we first convert it to a BCD file. Therefore, there has always been the question of how round-off would affect other users.

Critical assembly ZPR-67 has been computed using a binary LIB-V and again using a BCD LIB-V. The results from both cases are the same to four decimal places for all parameters. Therefore, round-off has no significant effect. Furthermore, to make sure Los Alamos is on the same footing as other laboratories that receive LIB-V, Los Alamos now uses in its calculations precisely the same data that is sent out.

TABLE III

UNCORRECTED EIGENVALUES

Critical	SUPERX	1DX	SUPERX-1DX
JEZEBEL	0.9600	0.9615	- 0.0015
VERA11A	0.9441	0.9543	- 0.0102
ZPR348	0.9829	0.9862	- 0.0033
ZEBRA3	0.9959	1.0037	- 0.0078
GODIVA	0.9666	0.9686	- 0.0020
VERA1B	0.9705	0.9579	+ 0.0126
ZPR36F	0.9915	0.9969	- 0.0054
ZPR311	1.0062	1.0115	- 0.0053
ZPR312	0.9963	0.9968	- 0.0005
ZEBRA2	0.9956	0.9771	+ 0.0185
ZPPR2	0.9817	0.9835	- 0.0018
ZPR67	0.9824	0.9835	- 0.0011
ZPR356B	1.0039	1.0059	- 0.0020
ZPR66A	0.9843	0.9808	+ 0.0035
SNEAK7A	0.9944	0.9978	- 0.0034
SNEAK7B	1.0001	1.0054	- 0.0053

D. Elastic Scattering Correction in TRANSX (R. E. MacFarlane)

Multigroup cross sections are produced using a model for the shape of the flux inside the group. If the actual flux in a system being analyzed with these cross sections is different from the model flux, a substantial error in the elastic removal cross section can result for the heavier materials since all of the removal comes from the bottom portion of the group.

The removal from group g to group g' can be written

$$R^{M}_{g\to g'} = \int_g du \int_{g'} du' \; \sigma_e \; (u\to u') \; \phi^M(u) \quad ,$$

where u is lethargy, σ_e is the elastic scattering differential cross section, and ϕ^M is the model flux. If the actual flux at the bottom of the group has a different slope than the model flux,

$$\phi(u) = [a-b\;(u_g-u)]\;\phi^M(u) \quad ,$$

where u_g is the lethargy at the bottom of group g. The removal rate becomes

$$R_{g\to g'} = R^M_{g\to g'}\;[a-b\gamma_{g\to g'}] \quad ,$$

where

$$\gamma_{g\to g'} = \frac{\int_g du \int_{g'} du \;(u_g-u)\;\sigma_e\;(u\to u')\;\phi^M(u)}{\int_g du_{g'} \int du' \;\sigma_e\;(u\to u')\;\phi^M(u)} \quad .$$

The quantity $\gamma_g = \Sigma_{g'}\gamma_{g\to g'}$ is already available on the MATXS library. If this value of γ is used for all groups and Legendre orders, an appropriate correction of the elastic scattering matrix elements can be made.

However, it is difficult to estimate the value a and slope b of the flux ratio at the bottom of the group from a computed multigroup flux because the ratio ϕ/ϕ^M normally contains some residual resonance effects. It is essentially impossible to guess the flux shape if only one or two groups of the ratio show the resonance effect. Nevertheless, the smooth trend in the ratio over several groups can be determined, and the corresponding trend in the elastic scattering correction will lead to improved values for averages like k_{eff} and reaction rate ratios even though the flux may not be improved near a resonance.

It is assumed that the smoothed flux ratio can be represented by

$$\ln(\phi/\phi^M) = \chi_0 + \chi_1(u_i-u) + \chi_2(u_i-u)^2$$

in the region of lethary u_i. The coefficients are computed using a least-squares fit to six values of the ratio assigned to the lethargy center of each of the six groups (three above u_g and three below). The parameters a and b are determined at the bottom of the group, and the smoothed value of the ratio at the center of the group is used to find the change in cross section that will give the desired change in removal rate.

This method is very stable. It avoids the divergences in removal cross section often seen with other methods while still providing a significant improvement in computed integral properties for typical fast-reactor benchmarks. It is included in the new version of TRANSX available on the mass Los Alamos storage directory /TRANSX as S3 (source) and X3 (executable).

E. A Format for Charged-Particle Induced Reactions (R. E. MacFarlane, P. G. Young, G. M. Hale, and L. Stewart)

The Evaluated Nuclear Data File (ENDF/B) is currently dominated by neutron and photon data. However, new applications such as fusion-reactor analysis, fusion-material radiation damage and activation, and particle-beam cancer therapy are creating increased demands for cross sections and energy-angle distributions of secondary particles for reactions induced by charged particles. The Cross Section Evaluation Working Group (CSEWG) has established a Charged-Particle Data Subcommittee to develop formats and procedures for adding such data to the ENDF/B system.

During this quarter, a format proposal has been constructed and distributed to members of the committee. The proposal describes reactions by giving the production cross section σ_i for each reaction product in the form

$$\sigma_i(\mu,E\rightarrow E') = \sigma(E)y_i(E)f_i(\mu,E\rightarrow E')/2\pi \quad ,$$

where i denotes one particular product, E is the incident particle energy, μ is the scattering cosine, σ is the interaction cross section, y_i is the yield or multiplicity of the product, and f_i is the normalized distribution of the product in angle and energy. Other quantities such as Maxwellian-averaged cross sections, in-flight reaction rates, activation, transmutation, gas production,

and radiation damage are considered to be derived quantities and would be produced from the primary file using a processing code.

Reaction nomenclature is based on the conventional form

target (projectile, products) residual.

The different combinations of target and projectile are treated as different materials and given unique MAT numbers. Reaction MT values are reserved for the common one-, two-, and three-particle reactions, but many-particle reactions and complex sums of reactions can be included without loss of detail using special summation MT values.

The format for cross sections is similar to the existing File 3 except that a new interpolation scheme is provided to represent the effects of the Coulomb penetrabilities near thresholds. The section that contains product yields is analogous to File 12 or to the $\bar{\nu}$ records in File 1 except that it contains subsections for every product. This allows the file to describe isomer production, transmutation, and the complex sum of reactions normally seen at high energies.

The file used to describe product distributions has a special format for elastic scattering of charged particles including the effects of Coulomb scattering. Angular distributions for other two-body channels are given in a way similar to that used in File 4. Products of multi-body reactions are described using correlated energy-angle distributions because such correlations are known to be important for the light isotopes and at high energies. A special two-dimensional interpolation scheme called "the method of corresponding points" is provided to allow smooth interpolation along the contours of a function rather than jagged steps along E and E'.

This format is general enough to allow the full detail of a nuclear-model calculation to be stored, but it also has defaults appropriate for the direct inclusion of evaluated experimental data. It offers the hope of a dramatic improvement in the availability of reliable data to the charged-particle community.

F. Calculations in Support of ISNF [R. J. LaBauve, D. C. George, and P. D. Soran (X-6)]

Discrete ordinates calculations in support of National Bureau of Standard's Intermediate Energy Standard Neutron Flux (ISNF) facility were completed during this reporting period. These calculations were in addition to those reported in Ref. 27 and were necessitated mainly by remeasurement of the ISNF configuration.

The most recent ISNF specifications, ISNF-3, are shown in Fig. 13. The ISNF-CV configuration, which was also included among the calculations, is the ISNF with the boron shell and its aluminum cap removed (ISNF-4).

The discrete calculations were performed with the ONEDANT code[28] using cross-section input processed from ENDF/B-V by the NJOY code[29] in both 70 and 150 neutron energy groups. The 70-group set is one generated at LASL and denoted as LIB-V.[30]

It has been used extensively in the calculation of fast-reactor benchmarks. These experiments usually have maximum flux below 1.5 MeV, so the group boundaries of the 70-group set have been selected to give the most detail in this region. Also, the weighting function used in generating the 70-group set was tailored to best represent the spectra of these fast critical systems. The ISNF spectrum, on the other hand, approximates a fission spectrum having a maximum at about 1.5 MeV, so the 70-group structure is not ideal for ISNF calculations. The energy boundaries of the 70-group set are given in Table IV.

The 150 energy group structure shown in Table V was specifically designed for ISNF calculations. As can be seen in this Table, a minimum lethargy width of 0.025 occurs from 0.6 to 2.7 MeV in this set. Also, the NBS 53-group structure is a sub-set of the 150 groups, as indicated in the table. Both the 70-group and 150-group sets are of Legendre order P_3.

Discrete ordinates calculations (S_8) performed with the ONEDANT code are shown in Table VI. Central flux/lethargy for the ISNF in 70 groups and 150 groups are shown in Figs. 14-16, respectively. The percent differences between calculations using the ENDF/B-V ^{235}U fission spectrum and those with the NBS ^{235}U fission spectrum for these three cases are shown in Figs. 17-19. The central fluxes for all six cases were sent to NBS on punched cards.

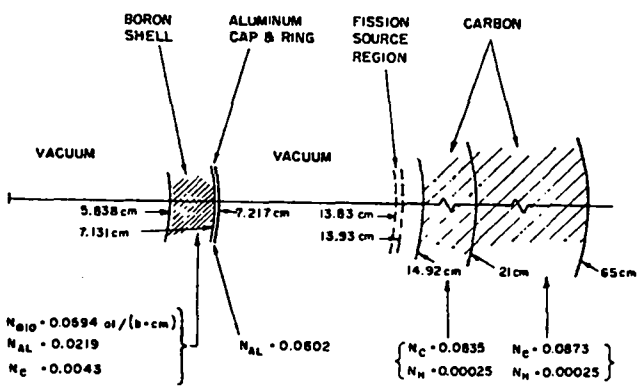

Fig. 13.
Physical parameters for ISNF-3 and ISNF-4.

TABLE IV

BOUNDARIES FOR 70-GROUP CROSS-SECTION SET

GRP NO.	E-HI	E-LO	U-LO	U-HI	U-WIDTH
1	.2000E+08	.1649E+08	-.6931E+00	-.5000E+00	.193
2	.1649E+08	.1284E+08	-.5000E+00	-.2500E+00	.250
3	.1284E+08	.1000E+08	-.2500E+00	0.	.250
4	.1000E+08	.7788E+07	0.	.2500E+00	.250
5	.7788E+07	.6065E+07	.2500E+00	.5000E+00	.250
6	.6065E+07	.4724E+07	.5000E+00	.7500E+00	.250
7	.4724E+07	.3679E+07	.7500E+00	.1000E+01	.250
8	.3679E+07	.2865E+07	.1000E+01	.1250E+01	.250
9	.2865E+07	.2231E+07	.1250E+01	.1500E+01	.250
10	.2231E+07	.1738E+07	.1500E+01	.1750E+01	.250
11	.1738E+07	.1353E+07	.1750E+01	.2000E+01	.250
12	.1353E+07	.1194E+07	.2000E+01	.2125E+01	.125
13	.1194E+07	.1054E+07	.2125E+01	.2250E+01	.125
14	.1054E+07	.9302E+06	.2250E+01	.2375E+01	.125
15	.9302E+06	.8209E+06	.2375E+01	.2500E+01	.125
16	.8209E+06	.7244E+06	.2500E+01	.2625E+01	.125
17	.7244E+06	.6393E+06	.2625E+01	.2750E+01	.125
18	.6393E+06	.5642E+06	.2750E+01	.2875E+01	.125
19	.5642E+06	.4979E+06	.2875E+01	.3000E+01	.125
20	.4979E+06	.4394E+06	.3000E+01	.3125E+01	.125
21	.4394E+06	.3877E+06	.3125E+01	.3250E+01	.125
22	.3877E+06	.3020E+06	.3250E+01	.3500E+01	.250
23	.3020E+06	.2352E+06	.3500E+01	.3750E+01	.250
24	.2352E+06	.1832E+06	.3750E+01	.4000E+01	.250
25	.1832E+06	.1426E+06	.4000E+01	.4250E+01	.250
26	.1426E+06	.1111E+06	.4250E+01	.4500E+01	.250
27	.1111E+06	.8652E+05	.4500E+01	.4750E+01	.250
28	.8652E+05	.6738E+05	.4750E+01	.5000E+01	.250
29	.6738E+05	.5248E+05	.5000E+01	.5250E+01	.250
30	.5248E+05	.4087E+05	.5250E+01	.5500E+01	.250
31	.4087E+05	.3183E+05	.5500E+01	.5750E+01	.250
32	.3183E+05	.2809E+05	.5750E+01	.5875E+01	.125
33	.2809E+05	.2479E+05	.5875E+01	.6000E+01	.125
34	.2479E+05	.2188E+05	.6000E+01	.6125E+01	.125
35	.2188E+05	.1931E+05	.6125E+01	.6250E+01	.125
36	.1931E+05	.1704E+05	.6250E+01	.6375E+01	.125
37	.1704E+05	.1503E+05	.6375E+01	.6500E+01	.125
38	.1503E+05	.1327E+05	.6500E+01	.6625E+01	.125
39	.1327E+05	.1171E+05	.6625E+01	.6750E+01	.125
40	.1171E+05	.1033E+05	.6750E+01	.6875E+01	.125
41	.1033E+05	.9119E+04	.6875E+01	.7000E+01	.125
42	.9119E+04	.8047E+04	.7000E+01	.7125E+01	.125
43	.8047E+04	.7102E+04	.7125E+01	.7250E+01	.125
44	.7102E+04	.6267E+04	.7250E+01	.7375E+01	.125
45	.6267E+04	.5531E+04	.7375E+01	.7500E+01	.125
46	.5531E+04	.4881E+04	.7500E+01	.7625E+01	.125
47	.4881E+04	.4307E+04	.7625E+01	.7750E+01	.125
48	.4307E+04	.3801E+04	.7750E+01	.7875E+01	.125
49	.3801E+04	.3355E+04	.7875E+01	.8000E+01	.125
50	.3355E+04	.2961E+04	.8000E+01	.8125E+01	.125
51	.2961E+04	.2613E+04	.8125E+01	.8250E+01	.125
52	.2613E+04	.2306E+04	.8250E+01	.8375E+01	.125
53	.2306E+04	.2035E+04	.8375E+01	.8500E+01	.125
54	.2035E+04	.1796E+04	.8500E+01	.8625E+01	.125
55	.1796E+04	.1585E+04	.8625E+01	.8750E+01	.125
56	.1585E+04	.1398E+04	.8750E+01	.8875E+01	.125
57	.1398E+04	.1234E+04	.8875E+01	.9000E+01	.125
58	.1234E+04	.1089E+04	.9000E+01	.9125E+01	.125
59	.1089E+04	.9611E+03	.9125E+01	.9250E+01	.125
60	.9611E+03	.7485E+03	.9250E+01	.9500E+01	.250
61	.7485E+03	.5830E+03	.9500E+01	.9750E+01	.250
62	.5830E+03	.4540E+03	.9750E+01	.1000E+02	.250
63	.4540E+03	.3536E+03	.1000E+02	.1025E+02	.250
64	.3536E+03	.2754E+03	.1025E+02	.1050E+02	.250
65	.2754E+03	.2145E+03	.1050E+02	.1075E+02	.250
66	.2145E+03	.1670E+03	.1075E+02	.1100E+02	.250
67	.1670E+03	.1301E+03	.1100E+02	.1125E+02	.250
68	.1301E+03	.1013E+03	.1125E+02	.1150E+02	.250
69	.1013E+03	.6144E+02	.1150E+02	.1200E+02	.500
70	.6144E+02	.1068E+02	.1200E+02	.1375E+02	1.750

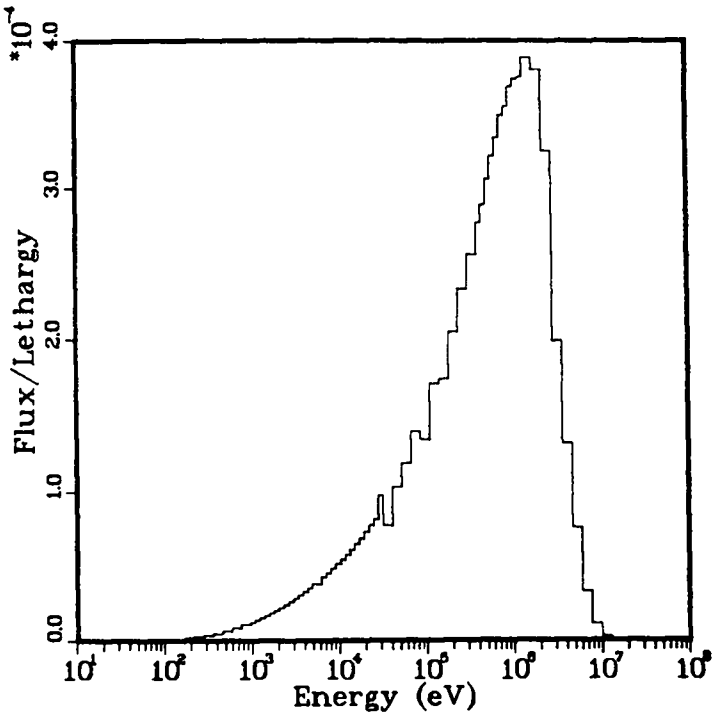

Fig. 14.
ISNF central spectrum in 70 groups.

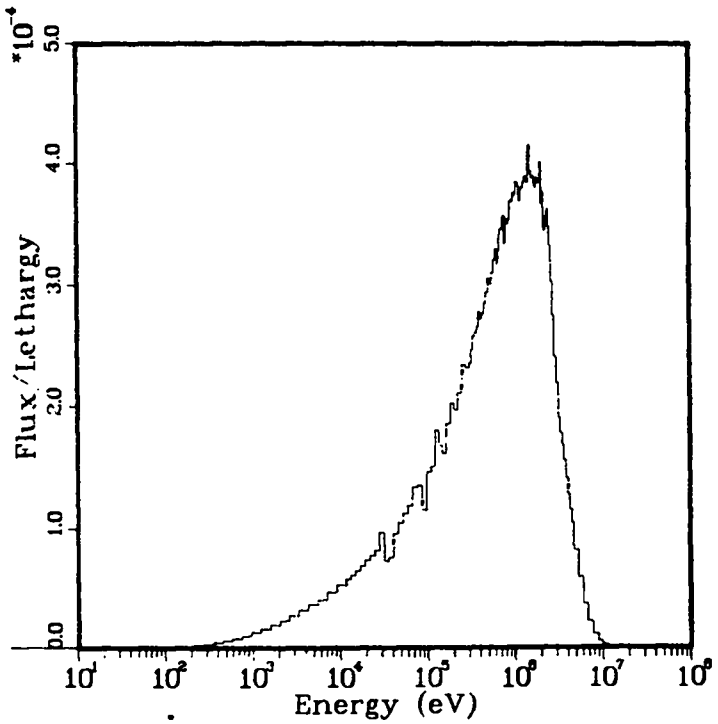

Fig. 15.
ISNF central spectrum in 150 groups.

TABLE V

BOUNDARIES FOR 150-GROUP CROSS-SECTION SET
(* denotes bounds of 53-group NBS set)

1	.2000E+08*	.1822E+08*	-.6931E+00	-.6000E+00	.093
2	.1822E+08*	.1492E+08*	-.6000E+00	-.4000E+00	.200
3	.1492E+08*	.1317E+08	-.4000E+00	-.2750E+00	.125
4	.1317E+08	.1162E+08*	-.2750E+00	-.1500E+00	.125
5	.1162E+08*	.1000E+08	-.1500E+00	0.	.150
6	.1000E+08	.9048E+07*	0.	.1000E+00	.100
7	.9048E+07*	.7788E+07	.1000E+00	.2500E+00	.150
8	.7788E+07	.6873E+07*	.2500E+00	.3750E+00	.125
9	.6873E+07*	.6065E+07*	.3750E+00	.5000E+00	.125
10	.6065E+07*	.5353E+07	.5000E+00	.6250E+00	.125
11	.5353E+07	.4724E+07*	.6250E+00	.7500E+00	.125
12	.4724E+07*	.4493E+07	.7500E+00	.8000E+00	.050
13	.4493E+07	.4274E+07	.8000E+00	.8500E+00	.050
14	.4274E+07	.4066E+07	.8500E+00	.9000E+00	.050
15	.4066E+07	.3867E+07	.9000E+00	.9500E+00	.050
16	.3867E+07	.3679E+07*	.9500E+00	.1000E+01	.050
17	.3679E+07*	.3499E+07	.1000E+01	.1050E+01	.050
18	.3499E+07	.3329E+07	.1050E+01	.1100E+01	.050
19	.3329E+07	.3166E+07*	.1100E+01	.1150E+01	.050
20	.3166E+07*	.3012E+07	.1150E+01	.1200E+01	.050
21	.3012E+07	.2865E+07	.1200E+01	.1250E+01	.050
22	.2865E+07	.2725E+07*	.1250E+01	.1300E+01	.050
23	.2725E+07*	.2658E+07	.1300E+01	.1325E+01	.025
24	.2658E+07	.2592E+07	.1325E+01	.1350E+01	.025
25	.2592E+07	.2528E+07	.1350E+01	.1375E+01	.025
26	.2528E+07	.2466E+07*	.1375E+01	.1400E+01	.025
27	.2466E+07*	.2405E+07	.1400E+01	.1425E+01	.025
28	.2405E+07	.2346E+07	.1425E+01	.1450E+01	.025
29	.2346E+07	.2288E+07	.1450E+01	.1475E+01	.025
30	.2288E+07	.2231E+07*	.1475E+01	.1500E+01	.025
31	.2231E+07*	.2176E+07	.1500E+01	.1525E+01	.025
32	.2176E+07	.2122E+07	.1525E+01	.1550E+01	.025
33	.2122E+07	.2070E+07	.1550E+01	.1575E+01	.025
34	.2070E+07	.2019E+07	.1575E+01	.1600E+01	.025
35	.2019E+07	.1969E+07	.1600E+01	.1625E+01	.025
36	.1969E+07	.1921E+07	.1625E+01	.1650E+01	.025
37	.1921E+07	.1873E+07*	.1650E+01	.1675E+01	.025
38	.1873E+07*	.1827E+07	.1675E+01	.1700E+01	.025
39	.1827E+07	.1782E+07	.1700E+01	.1725E+01	.025
40	.1782E+07	.1738E+07	.1725E+01	.1750E+01	.025
41	.1738E+07	.1695E+07	.1750E+01	.1775E+01	.025
42	.1695E+07	.1653E+07	.1775E+01	.1800E+01	.025
43	.1653E+07	.1612E+07*	.1800E+01	.1825E+01	.025
44	.1612E+07*	.1572E+07	.1825E+01	.1850E+01	.025
45	.1572E+07	.1534E+07	.1850E+01	.1875E+01	.025
46	.1534E+07	.1496E+07	.1875E+01	.1900E+01	.025
47	.1496E+07	.1459E+07	.1900E+01	.1925E+01	.025
48	.1459E+07	.1423E+07	.1925E+01	.1950E+01	.025
49	.1423E+07	.1388E+07	.1950E+01	.1975E+01	.025
50	.1388E+07	.1353E+07*	.1975E+01	.2000E+01	.025
51	.1353E+07*	.1320E+07	.2000E+01	.2025E+01	.025
52	.1320E+07	.1287E+07	.2025E+01	.2050E+01	.025
53	.1287E+07	.1256E+07	.2050E+01	.2075E+01	.025
54	.1256E+07	.1225E+07	.2075E+01	.2100E+01	.025
55	.1225E+07	.1194E+07	.2100E+01	.2125E+01	.025
56	.1194E+07	.1165E+07	.2125E+01	.2150E+01	.025
57	.1165E+07	.1136E+07	.2150E+01	.2175E+01	.025
58	.1136E+07	.1108E+07*	.2175E+01	.2200E+01	.025
59	.1108E+07*	.1081E+07	.2200E+01	.2225E+01	.025
60	.1081E+07	.1054E+07	.2225E+01	.2250E+01	.025
61	.1054E+07	.1028E+07	.2250E+01	.2275E+01	.025
62	.1028E+07	.1003E+07	.2275E+01	.2300E+01	.025
63	.1003E+07	.9778E+06	.2300E+01	.2325E+01	.025
64	.9778E+06	.9616E+06*	.2325E+01	.2342E+01	.017
65	.9616E+06*	.9301E+06	.2342E+01	.2375E+01	.033
66	.9301E+06	.9072E+06	.2375E+01	.2400E+01	.025
67	.9072E+06	.8848E+06	.2400E+01	.2425E+01	.025
68	.8848E+06	.8629E+06	.2425E+01	.2450E+01	.025
69	.8629E+06	.8416E+06	.2450E+01	.2475E+01	.025
70	.8416E+06	.8209E+06*	.2475E+01	.2500E+01	.025
71	.8209E+06*	.8006E+06	.2500E+01	.2525E+01	.025
72	.8006E+06	.7808E+06	.2525E+01	.2550E+01	.025
73	.7808E+06	.7615E+06	.2550E+01	.2575E+01	.025
74	.7615E+06	.7427E+06	.2575E+01	.2600E+01	.025
75	.7427E+06	.7244E+06	.2600E+01	.2625E+01	.025

TABLE V (cont.)

76	.7244E+06	.7065E+06	.2625E+01	.2650E+01	.025
77	.7065E+06	.6891E+06	.2650E+01	.2675E+01	.025
78	.6891E+06	.6721E+06*	.2675E+01	.2700E+01	.025
79	.6721E+06*	.6555E+06	.2700E+01	.2725E+01	.025
80	.6555E+06	.6393E+06	.2725E+01	.2750E+01	.025
81	.6393E+06	.6235E+06	.2750E+01	.2775E+01	.025
82	.6235E+06	.6081E+06	.2775E+01	.2800E+01	.025
83	.6081E+06	.5784E+06	.2800E+01	.2850E+01	.050
84	.5784E+06	.5502E+06	.2850E+01	.2900E+01	.050
85	.5502E+06	.5234E+06	.2900E+01	.2950E+01	.050
86	.5234E+06	.4979E+06*	.2950E+01	.3000E+01	.050
87	.4979E+06*	.4736E+06	.3000E+01	.3050E+01	.050
88	.4736E+06	.4505E+06	.3050E+01	.3100E+01	.050
89	.4505E+06	.4285E+06	.3100E+01	.3150E+01	.050
90	.4285E+06	.4076E+06*	.3150E+01	.3200E+01	.050
91	.4076E+06*	.3877E+06	.3200E+01	.3250E+01	.050
92	.3877E+06	.3688E+06	.3250E+01	.3300E+01	.050
93	.3688E+06	.3508E+06	.3300E+01	.3350E+01	.050
94	.3508E+06	.3337E+06	.3350E+01	.3400E+01	.050
95	.3337E+06	.3175E+06	.3400E+01	.3450E+01	.050
96	.3175E+06	.3020E+06*	.3450E+01	.3500E+01	.050
97	.3020E+06*	.2732E+06	.3500E+01	.3600E+01	.100
98	.2732E+06	.2472E+06	.3600E+01	.3700E+01	.100
99	.2472E+06	.2237E+06*	.3700E+01	.3800E+01	.100
100	.2237E+06*	.2024E+06	.3800E+01	.3900E+01	.100
101	.2024E+06	.1832E+06*	.3900E+01	.4000E+01	.100
102	.1832E+06*	.1657E+06	.4000E+01	.4100E+01	.100
103	.1657E+06	.1500E+06	.4100E+01	.4200E+01	.100
104	.1500E+06	.1357E+06*	.4200E+01	.4300E+01	.100
105	.1357E+06*	.1228E+06	.4300E+01	.4400E+01	.100
106	.1228E+06	.1111E+06*	.4400E+01	.4500E+01	.100
107	.1111E+06*	.9804E+05	.4500E+01	.4625E+01	.125
108	.9804E+05	.8652E+05*	.4625E+01	.4750E+01	.125
109	.8652E+05*	.7635E+05	.4750E+01	.4875E+01	.125
110	.7635E+05	.6738E+05*	.4875E+01	.5000E+01	.125
111	.6738E+05*	.5946E+05	.5000E+01	.5125E+01	.125
112	.5946E+05	.5248E+05*	.5125E+01	.5250E+01	.125
113	.5248E+05*	.4631E+05	.5250E+01	.5375E+01	.125
114	.4631E+05	.4087E+05*	.5375E+01	.5500E+01	.125
115	.4087E+05*	.3607E+05	.5500E+01	.5625E+01	.125
116	.3607E+05	.3183E+05*	.5625E+01	.5750E+01	.125
117	.3183E+05*	.2809E+05	.5750E+01	.5875E+01	.125
118	.2809E+05	.2479E+05*	.5875E+01	.6000E+01	.125
119	.2479E+05*	.2187E+05	.6000E+01	.6125E+01	.125
120	.2187E+05	.1930E+05*	.6125E+01	.6250E+01	.125
121	.1930E+05*	.1704E+05	.6250E+01	.6375E+01	.125
122	.1704E+05	.1503E+05*	.6375E+01	.6500E+01	.125
123	.1503E+05*	.1327E+05	.6500E+01	.6625E+01	.125
124	.1327E+05	.1171E+05*	.6625E+01	.6750E+01	.125
125	.1171E+05*	.9119E+04*	.6750E+01	.7000E+01	.250
126	.9119E+04*	.7102E+04	.7000E+01	.7250E+01	.250
127	.7102E+04	.5531E+04*	.7250E+01	.7500E+01	.250
128	.5531E+04*	.4307E+04	.7500E+01	.7750E+01	.250
129	.4307E+04	.3355E+04*	.7750E+01	.8000E+01	.250
130	.3355E+04*	.2613E+04	.8000E+01	.8250E+01	.250
131	.2613E+04	.2035E+04*	.8250E+01	.8500E+01	.250
132	.2035E+04*	.1585E+04	.8500E+01	.8750E+01	.250
133	.1585E+04	.1234E+04*	.8750E+01	.9000E+01	.250
134	.1234E+04*	.9611E+03	.9000E+01	.9250E+01	.250
135	.9611E+03	.7485E+03*	.9250E+01	.9500E+01	.250
136	.7485E+03*	.5829E+03	.9500E+01	.9750E+01	.250
137	.5829E+03	.4540E+03*	.9750E+01	.1000E+02	.250
138	.4540E+03*	.3536E+03	.1000E+02	.1025E+02	.250
139	.3536E+03	.2754E+03*	.1025E+02	.1050E+02	.250
140	.2754E+03*	.2145E+03	.1050E+02	.1075E+02	.250
141	.2145E+03	.1670E+03*	.1075E+02	.1100E+02	.250
142	.1670E+03*	.1013E+03*	.1100E+02	.1150E+02	.500
143	.1013E+03*	.6144E+02*	.1150E+02	.1200E+02	.500
144	.6144E+02*	.3727E+02*	.1200E+02	.1250E+02	.500
145	.3727E+02*	.1371E+02*	.1250E+02	.1350E+02	1.000
146	.1371E+02*	.8315E+01*	.1350E+02	.1400E+02	.500
147	.8315E+01*	.2382E+01*	.1400E+02	.1525E+02	1.250
148	.2382E+01*	.8764E+00*	.1525E+02	.1625E+02	1.000
149	.8764E+00*	.4140E+00*	.1625E+02	.1700E+02	.750
150	.4140E+00*	.1523E+00*	.1700E+02	.1800E+02	1.000

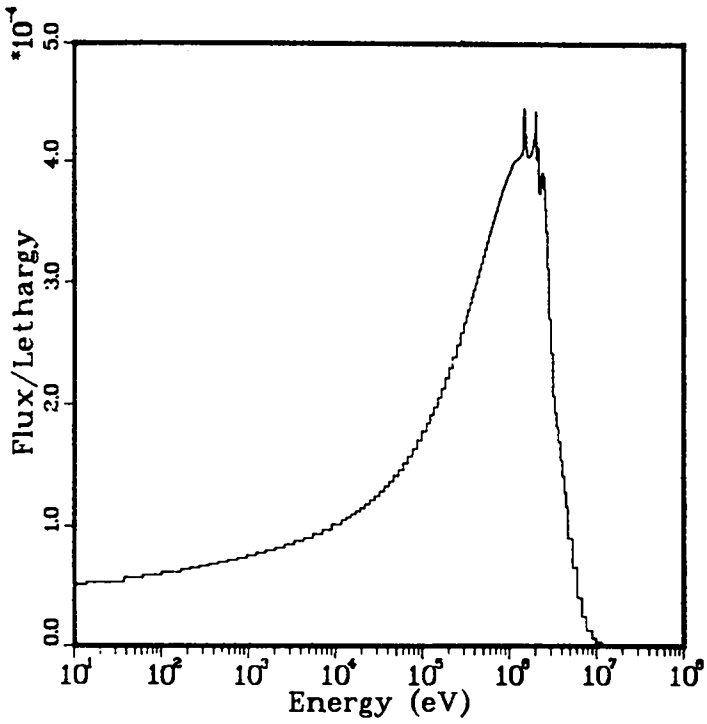

Fig. 16.
ISNF-CV central spectrum in 150 groups.

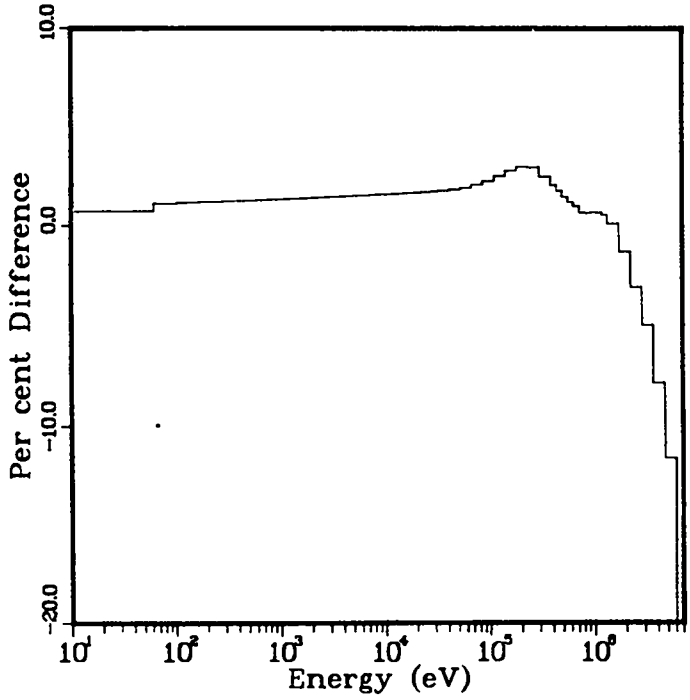

Fig. 17.
Comparison of 70-group ISNF calculations using ENDF/B-V and NBS ^{235}U thermal fission spectra.

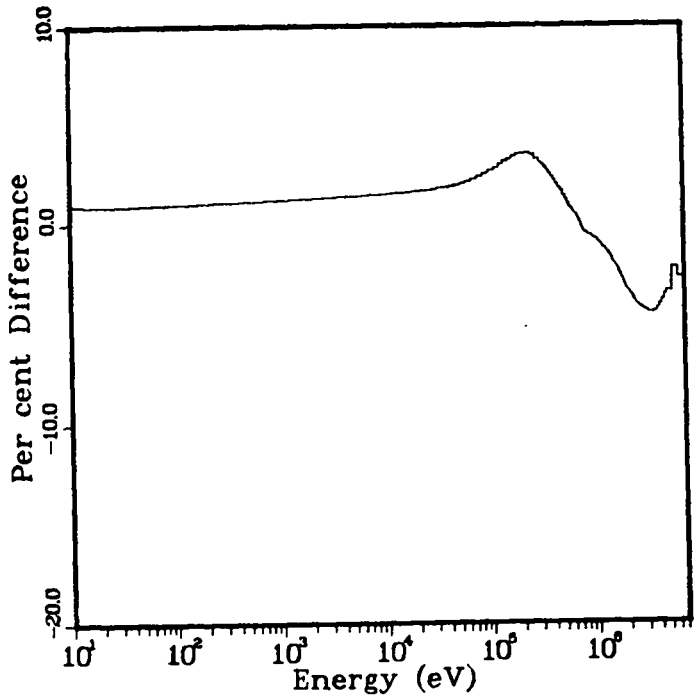

Fig. 18.
Comparison of 150-group ISNF calculations using ENDF/B-V and NBS ^{235}U thermal fission spectra.

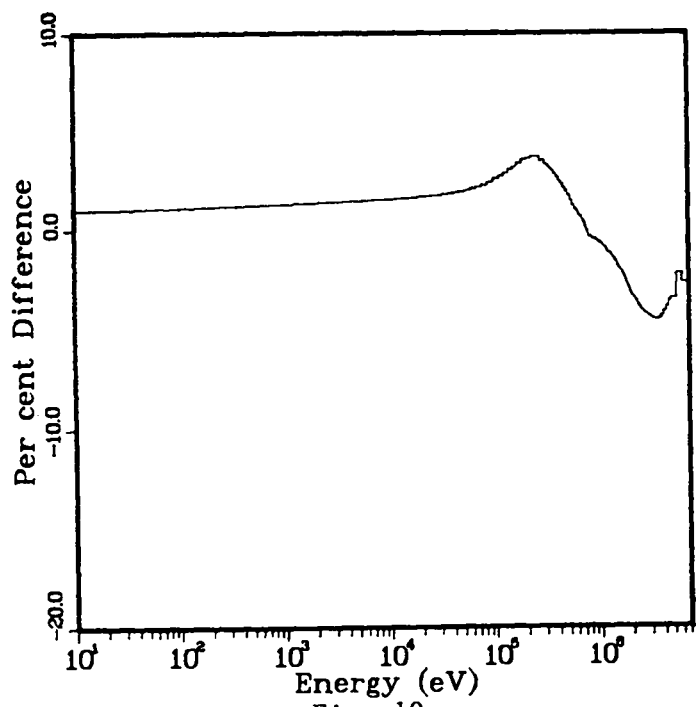

Fig. 19.
Comparison of 150-group ISNF-CV calculations using ENDF/B-V and NBS ^{235}U thermal fission spectra.

TABLE VI

DISCRETE ORDINATES CALCULATIONS (S_8) FOR ISNF

Configuration	Cross-Section Set	^{235}U Thermal Fission Spectrum
ISNF	70-group	ENDF/B-V
ISNF	70-group	NBS
ISNF	150-group	ENDF/B-V
ISNF	150-group	NBS
ISNF-CV	150-group	ENDF/B-V
ISNF-CV	150-group	NBS

G. Compact Representation of Neutron Activation and Decay Data: Neutron-Reaction Effects (D. W. Muir)

In Ref. 31 we described a method for constructing a calculation-oriented nuclear-data library intended to describe as compactly as possible neutron activation and decay and decay processes in "decay-dominated" applications. It was assumed there that neutron reactions could be entirely neglected, in comparison with radioactive decay, when calculating the rates of depletion and transmutation of all radioactive species present.

Here we describe an extension of that method to treat in an approximate manner finite neutron-reaction effects, still within the framework of the decoupled decay equations discussed in Ref. 31. One important application of this extended method is to estimate the error incurred by neglecting neutron reactions. If use of the extended method in some particular case reveals that reaction effects are truly significant, one should complete the analysis using a more general buildup and depletion approach as implemented, for example, in the CINDER[32] program. In application areas where reactions cause only a small perturbation (and where the assumptions below are valid), the method described here can be used for the entire analysis.

In this development we assume that radionuclides are depleted and transmuted primarily by neutrons with some fixed energy (or with some fixed energy spectrum). This assumption would be valid, for example, in the common situation where thermal-neutron reactions predominate. We shall use the symbol ϕ, without an energy index, to represent the component of the neutron flux that is responsible for radionuclide depletion and transmutation. We further assume that ϕ is approximately constant in time. (Even in cases where this latter assumption is not valid, the formalism described here may still be useful in estimating the importance of reaction effects.)

We now repeat the development of Ref. 31, except that a finite value of ϕ is assumed. Notation already defined in Ref. 31 will not be redefined here. The decay equations, Eq. (19) of Ref. 1 become

$$\frac{d}{dt}\underline{N} = \underline{D}_\phi \underline{N} \quad , \tag{1}$$

where the new matrix $\underline{D}_\phi$ is related to the previous $\underline{D}$ by $\underline{D}_\phi = \underline{D} + \phi \dot{\underline{D}}$. The diagonal element $\dot{d}_{ii}$ of $\dot{\underline{D}}$ is the destruction cross section of species X_i and the the off-diagonal element $\dot{d}_{ij}$ is the cross section for the transmutation of X_j into X_i. We do <u>not</u> need to restrict $\dot{\underline{D}}$ to the triangular form of $\underline{D}$.

The flux-dependent analog of the transformation (or diagonalization) matrix $\underline{A}$ of Ref. 1 satisfies, by the same arguments as given there, the equation

$$\underline{A}_\phi \underline{D}_\phi = \underline{D}^*_\phi \underline{A}_\phi \quad . \tag{2}$$

Since $\underline{D}_\phi$ is not triangular, we can no longer expect in general that the transformed decay constants (i.e., the elements of the diagonalized decay matrix $\underline{D}^*_\phi$) to be equal to the diagonal elements of $\underline{D}_\phi$. The determination of $\underline{D}^*_\phi$ becomes, in fact, a major part of the problem at hand.

Rather than proceeding immediately to solve Eq. (2) for $\underline{A}_\phi$ as we did in Ref. 1, it is more useful to differentiate Eq. (2) and solve for $\dot{\underline{A}}$, a matrix composed of the flux-derivatives of the elements of $\underline{A}_\phi$, all evaluated at $\phi = 0$. As shown below, $\dot{\underline{A}}$ can be used to generate $\dot{\underline{\Sigma}}^*$, which describes first-order flux-dependence of the cross sections for producing the various independent activities, and $\dot{\underline{S}}^*$, which describes the flux-dependence of the gamma-ray emission spectra of the independent activities. These problem-independent quantities $\dot{\underline{\Sigma}}^*$ and $\dot{\underline{S}}^*$ can be stored in the transformed activation and decay library along with their $\phi = 0$ counterparts $\underline{\Sigma}^*$ and $\underline{S}^*$. During the course of a radioactive-decay calculation, when macroscopic (region-dependent) cross sections are constructed from such a library, a region-dependent flux ϕ can be entered, and the needed flux-dependent activation ($\underline{\Sigma}^*_\phi$) and decay ($\underline{S}^*_\phi$) data can be generated as follows:

$$\underline{\Sigma}^*_\phi \simeq \underline{\Sigma}^* + \phi \dot{\underline{\Sigma}}^* \quad , \tag{3}$$

and

$$\underline{S}^*_\phi \simeq \underline{S}^* + \phi \dot{\underline{S}}^* \quad , \tag{4}$$

where Eqs. (3) and (4) are correct only to first order in ϕ.

In addition to $\dot{\underline{A}}$, which we need in order to generate $\dot{\underline{\Sigma}}^*$ and $\dot{\underline{S}}^*$ for use in Eqs. (3) and (4), we also require $\dot{\underline{D}}^*$, the flux-derivative of $\underline{D}^*_\phi$ at $\phi = 0$. $\dot{\underline{D}}^*$ can be used directly to generate the flux dependent decay constants,

$$\underline{D}^*_\phi \simeq \underline{D}^* + \phi\, \dot{\underline{D}}^* \quad , \tag{5}$$

again correct only to first order in ϕ.

To evaluate the needed flux-derivatives, we return to Eq. (2). Differentiating both sides with respect to ϕ and then setting $\phi = 0$ yields

$$\dot{\underline{A}}\, \underline{D} + \underline{A}\, \dot{\underline{D}} - \dot{\underline{D}}^*\, \underline{A} - \underline{D}^*\, \dot{\underline{A}} = 0 \quad . \tag{6}$$

Since $\underline{D}^*_\phi$ is by definition diagonal, $\dot{\underline{D}}^*$ is also diagonal. As in Ref. 31, we are free to set the normalization of $\underline{A}_\phi$, and we do so by requiring that $\underline{A}_\phi$ have a unit diagonal regardless of the magnitude of ϕ. This, in turn, implies that the diagonal elements of $\dot{\underline{A}}$ are all zero. By these considerations, we have reduced the numbers of unknowns in Eq. (6) from $2J^2$ to J^2, where J is the number of radioactive species that can be produced from the target material under consideration, i.e., the dimension of the square matrices $\underline{A}$ and $\underline{D}$. Equation (6) then reduces to a set of J^2 equations in J^2 unknowns, which we now solve.

It is convenient to relabel the (known) matrix product $\underline{A}\, \dot{\underline{D}}$ as $\underline{B}$. Further, let us introduce the notation $\alpha_{ij} \equiv (\dot{\underline{A}})_{ij}$, $b_{ij} \equiv (\underline{B})_{ij}$, and $\delta_{ij} \equiv (\dot{\underline{D}}^*)_{ij}$. If one writes out explicitly the ij-th element of the matrix obtained from the operations indicated in Eq. (6), one obtains the desired solution for the unknown α_{ij} and δ_{ij}. The solution takes on three basic forms, depending on whether $j > i$, $j = i$, or $j < i$.

<u>Case I. $(j > i)$</u>

$$\alpha_{ij} = \begin{cases} \dfrac{b_{ij}}{d_{ii} - d_{jj}} & \text{, if } j = J, \text{ and} \\[2ex] \dfrac{1}{d_{ii} - d_{jj}} \left(b_{ij} + \displaystyle\sum_{k=j+1}^{J} \alpha_{ik}\, d_{kj} \right) & \text{, if } j < J. \end{cases} \tag{7}$$

Case II. $(j = i)$

$$\delta_{ii} = \begin{cases} b_{ii}, \text{ if } i = J, \text{ and} \\ b_{ii} + \sum_{k=i+1}^{J} \alpha_{ik} d_{ki} \quad , \text{ if } i < J. \end{cases} \tag{8}$$

Case III. $(j < i)$

$$\alpha_{ij} = \frac{1}{d_{ii} - d_{jj}} \left(b_{ij} - \delta_{ii} a_{ij} + \sum_{\substack{k=j+1 \\ k \neq i}}^{J} \alpha_{ik} d_{kj} \right) \tag{9}$$

For a fixed row i, one can calculate all α_{ij} for which $j > i$ by applying Eq. (7) repeatedly, proceeding from high to low j-values; δ_{ii} can then be calculated from Eq. (8); finally, the remaining α_{ij} in row i can then be calculated from Eq. (9), again proceeding from high to low j-values. This completes the calculation of $\dot{\underline{A}}$ and $\dot{\underline{D}}^*$ in terms of the known quantities $\underline{A}$, $\underline{D}$, and $\dot{\underline{D}}$.

Finally, we show how $\dot{\underline{A}}$ can be used to generate $\dot{\underline{\Sigma}}^*$ and $\dot{\underline{S}}^*$. From Eq.(24) of Ref. 1

$$\underline{\Sigma}^*_\phi = \underline{A}_\phi \underline{\Sigma} \quad . \tag{10}$$

Differentiating with respect to ϕ, and then setting $\phi = 0$, we have at once

$$\dot{\underline{\Sigma}}^* = \dot{\underline{A}} \underline{\Sigma} \quad .$$

Similarly, from Eq. (29) of Ref. 1,

$$\underline{S}^*_\phi \underline{A}_\phi = \underline{S} \quad .$$

Again, differentiating at $\phi = 0$,

$$\dot{\underline{S}}^* \underline{A} + \underline{S}^* \dot{\underline{A}} = 0 \quad , \tag{11}$$

whence

$$\dot{\underline{S}}^* = - \underline{S}^* \dot{\underline{A}} \underline{A}^{-1} \quad . \tag{12}$$

As in the derivation of Eq. (31) of Ref. 31, the simple triangular form of $\underline{A}$ can be used to advantage in order to calculate $\dot{\underline{S}}^*$ without explicitly calculating $\underline{A}^{-1}$. If we return to Eq. (11) and label the (known) matrix product $\underline{S}^* \dot{\underline{A}}$ as $\underline{T}$, then one obtains immediately the following prescription for $\dot{\underline{S}}^*$. For m ranging over all gamma-ray energy groups,

$$\dot{s}^*_{mj} = \begin{cases} t_{mj} & , \text{ if } j = J, \\ t_{mj} - \sum_{k=j+1}^{J} \dot{s}^*_{mk} a_{kj}, & \text{if } j < J \quad . \end{cases} \tag{13}$$

III. FISSION PRODUCTS AND ACTINIDES: YIELDS, DECAY DATA, DEPLETION, AND BUILDUP

A. ENDF/B-V Data Libraries for CINDER Codes [T. R. England, W. B. Wilson, D. E. Wessol (EG&G, Idaho), N. L. Whittemore, and R. M. Boicourt]

Decay energies, yields, cross sections, and chains for fission products are now complete for CINDER-10[33] and CINDER-2, an evolved version of EPRI-CINDER.[34] Tests of CINDER-2 using the new data have not been made. Extensive tests of the larger CINDER-10 library have been made for fission-product decay power.

Cross sections for these codes were processed using the NJOY[29] code into 154 groups and collapsed to 4 groups using TOAFEW.[35] For decay data, multigroup spectra and various conservation tests of ENDF/B-V, a code SPEC5 was prepared. All ENDF/B-V MOD "0"[36] fission-product spectra have been processed into 158 groups. These include gamma + x ray, beta, positron, alpha, neutrino, and antineutrino spectra. Fission yields were processed using other codes as described in previous progress reports. An additional effort to augment the ENDF/B-V decay spectra is in progress.

Table VII lists the gross content of the ENDF/B-V fission-product files. These files require ≈ 105 000 records in ENDF/B-V format (3 461 413 octal words for storage) for the decay and cross-section files plus an additional ≈56 000 records for the yield files. Apart from descriptive information, there are

TABLE VII

GROSS CONTENT OF FISSION PRODUCT FILES

Quantity	Number
Total nuclides	877
Nuclides having cross sections[a]	196
Stable nuclides	127
Unstable nuclides[b]	750
Nuclides in isomeric states ($\geq$ 0.1 s)	154
Delayed neutron precursors	105
Nuclides having	
(1) one or more spectra	264
(2) electron spectra	233
(3) photon spectra	247
(4) positron or EC spectra	12
(5) conversion electron coefficients	157
(6) x-ray spectra	166
(7) discrete electron spectra	166
Fissionable nuclide yield sets[c]	20

[a] $\sigma(E)$ evaluations are complete (total, elastic, inelastic, capture, and angular distributions) from 10^{-5} eV to 20 MeV.

[b] Of these, 315 have decay energies derived from experiment, 264 being derived from decay spectra in the files.

[c] Each set contains ≈1200 direct and cumulative yields and uncertainties. The direct yields are values before delayed neutron emission and the cumulative values (by A and Z) apply after delayed neutron emission.

≈800 000 fields for the numerical entries, some being zero. The 60 actinides require a proportional number of numerical fields; processed multigroup cross sections for these, but not multigroup decay spectra, are complete.

Processing these files and forming and checking the CINDER libraries has been expensive and was a major task during this quarter.

B. ENDF/B-V Fission-Product Decay Power (T. R. England, W. B. Wilson, and N. L. Whittemore)

Using the new ENDF/B MOD "0"[36] CINDER-10[33] library, described in the previous section, the beta, gamma, and total decay powers have been calculated. Fission-product yields required special treatment to account for the differences in isomeric identifications, delayed neutron emission, and branching in the decay and yield files. Results have been compared to ENDF/B-IV including the total heating in the new ANS 5.1 Decay Power Standard.[37]

Decay following fission pulses have been used to emphasize differences between the ENDF/B-IV and -V fission-product files, shown in Fig. 20. There are large differences ($\pm$ 20% for ^{235}U and ≈30% for ^{239}Pu) at some cooling times.The reasons are being determined. For the pulse case there is concern particularly with gamma energies; these do not reproduce one experiment as well as did ENDF/B-IV. Tobias has found very similar results using the UK data base UKFPDD-2[38] and Yoshida finds nearly identical results using the October 1980 Japanese data JNDC.[39] Yoshida reports considerable improvement using estimated gamma and beta energies from Ref. 40 for nuclides having Q-values $\geq$ 5 MeV.

Most decay applications involve decay power following long irradiation times. For the case of equilibrium concentrations without neutron absorption effects, Fig. 21 compares the ENDF/B-V and ANS 5.1 Standard with ENDF/B-IV fission-product decay power. The standard represents the combined results of five experiments to 10^5 s and calculations using ENDF/B-IV for all longer times.[41] Differences at short times are not large for this case, and the large differences at long times are not of any practical concern.

These results, along with actinide decay power, have been submitted for presentation next June at the American Nuclear Society meeting in Miami, FL.

C. Iodine Release in Reactor Accidents (T. R. England and N. L. Whittemore)

The ENDF/B-IV and -V files have been used in many applications. A recent application was in support of Los Alamos and Oak Ridge research investigating iodine volatility in reactor accidents. In particular, when substantial amounts of water are present iodides tend to go into solution, particularly cesium iodide, greatly reducing the escape of iodine, as supported by the small iodine release following the TMI-2 accident. Using the ENDF/B data files and the CINDER code, we calculate that for all cooling and irradiation times of interest for the TMI-2 incident, there was ≈10 times more cesium produced than idodine, thus ensuring an abundant supply for formation of cesium iodide.

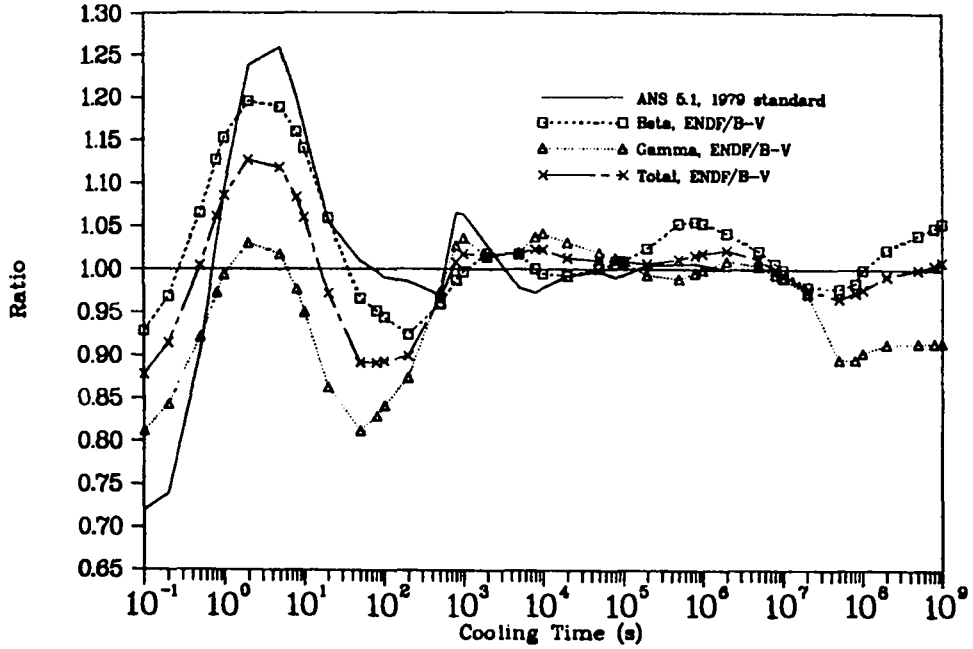

Fig. 20.
^{235}U thermal fission pulse comparison of ANS 5.1 and calculated ENDF/B-V fission-product decay powers as a ratio to ENDF/B-IV.

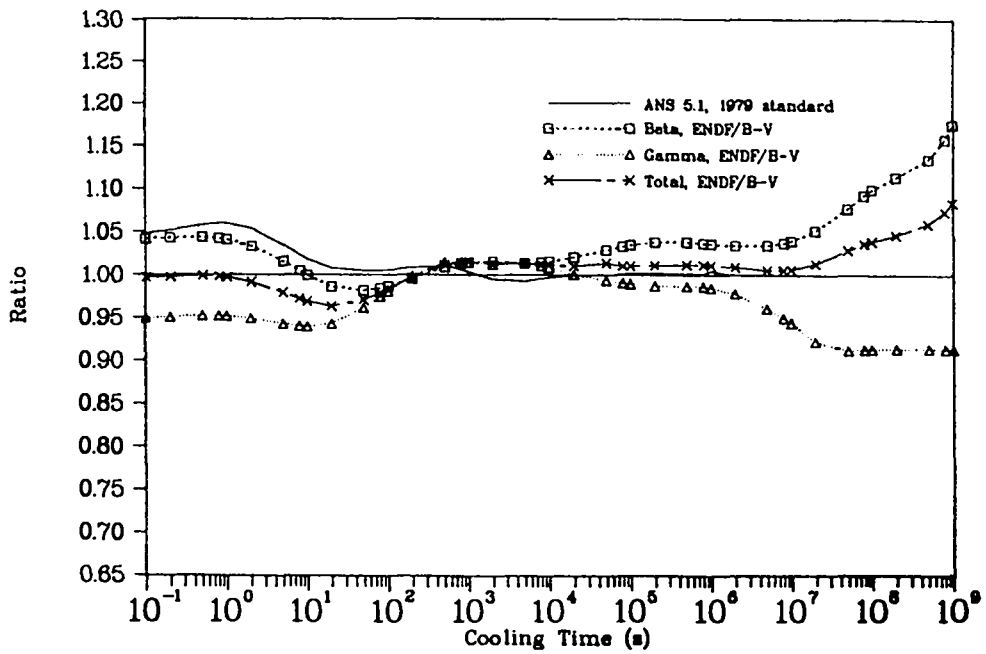

Fig. 21.
^{235}U thermal fission infinite comparison of ANS 5.1 and calculated ENDF/B-V fission-product decay powers as a ratio to ENDF/B-IV, 10^{13} s irradiation, no absorption.

D. Delayed Neutron Spectra [T. R. England, N. L. Whittemore, W. B. Wilson, and R. E. Schenter (HEDL)]

Using the ENDF/B-V fission yields and delayed neutron emission probabilities along with experimental precursor spectra, the combined spectra and delayed neutron yields were calculated for 11 fissionable nuclides at 1 or more fission neutron incident energies (20 cases). Spectra were grouped into the conventional six time groups. The total number of delayed neutrons was based on 105 precursors. The emission spectra are currently available (in 10 keV energy bins) for only 24 precursors, but these account for ≈80% of the delayed neutrons. The The integral of the calculated spectra was subsequently normalized to the total $\bar{\nu}_d$ calculated from all precursors.

Results for ^{235}U thermal fission are given in Fig. 22 prior to normalization. There are no precursors that have measured spectra in the shortest time group (group 6) nor or there any measured aggregate spectra for this group. (ENDF/B-V uses the shape of group 5 for group 6.)

All results were sent to Argonne National Laboratory for use in four ZPR critical calculations using diffusion theory and comparison results of the calculated spectra vs. ENDF/B-V and -IV evaluated spectra. The spectra for $^{235,238}U$ and $^{239-241}Pu$ fast fission were used normalized to the evaluated total. k_{eff}, β_{eff}, ℓ_p, and the reactivity conversion factor Ih/%Δk/k were compared. H. Henryson[42] (Argonne National Laboratory) reported the detailed comparisons; these show very small parameter differences between the use of calculated and ENDF/B-IV and -V evaluated aggregate spectra. This suggests that we can now calculate spectra for the many fissionable nuclides having no aggregate measured data. However, the accuracy of such calculations is strongly dependent on the quality of independent fission yields. The calculated spectra show more low-energy neutrons than the ENDF/B-V evaluated spectra. Recent hydrogen recoil measurements show still more low-energy neutrons. It therefore appears that calculated spectra are an improvement over current evaluations, at least for $^{235,238}U$ and $^{239-241}Pu$ fission, but that even the calculated spectra may significantly miss delayed neutrons having energies smaller than ≈50 keV. Nevertheless, the quality of the calculated spectra is impressive, is continuing to improve because of new precursor measurements, and will be a continuing area of research. Figure 23 shows a typical comparison of the ENDF/B-V evaluated equilibrium spectra and the calculated spectra.

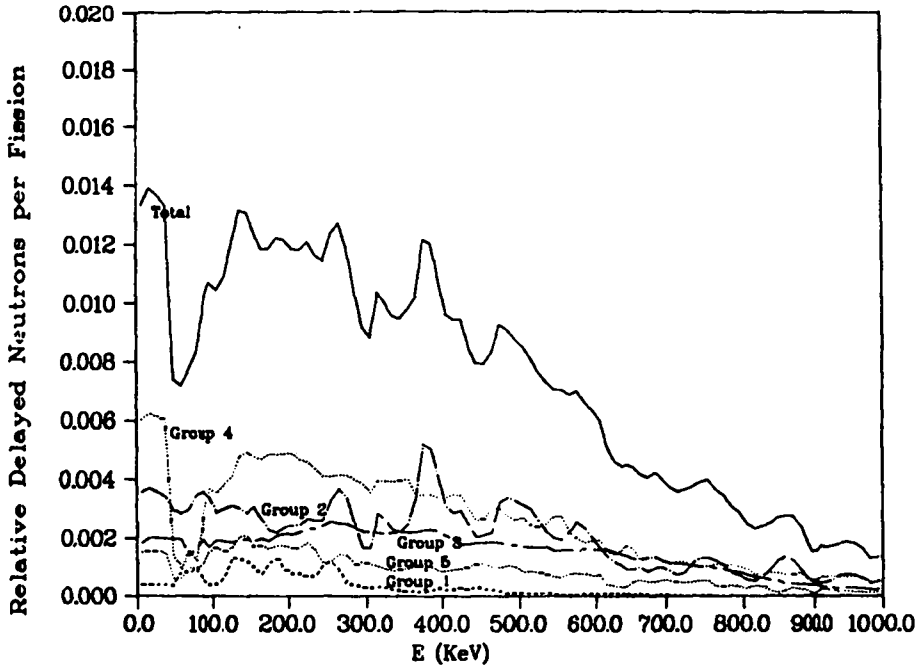

Fig. 22.
^{235}U delayed neutron group spectra based on 24 precursors and ENDF/B-V yields.

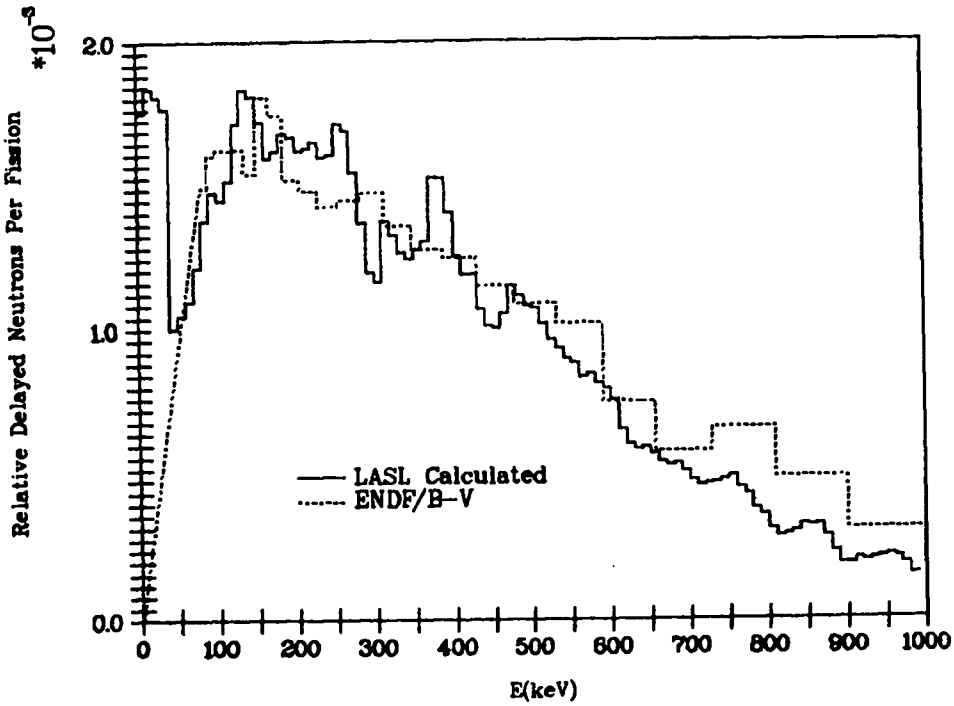

Fig. 23.
Comparison of calculated and ENDF/B-V evaluated delayed neutron spectra ^{235} thermal fission.

E. The $^{19}F(\alpha,n)$ Neutron Production From the Decay of U Nuclides in UF_6 [W. B. Wilson, J. E. Stewart (Q-1), and R. T. Perry (U. of Wisconsin)]

The production of neutrons from the interaction of U nuclide decay alpha particles with ^{19}F in UF_6 provides a neutron source for the passive monitoring of a gas centrifuge enrichment process. Our recent experience in the calculation of $^{17,18}O(\alpha,n)$ neutron production from actinide decay in oxide fuels[43–45] has facilitated the calculation of $^{19}F(\alpha,n)$ neutron production in UF_6.

The probability that an alpha particle of energy E_α will produce a neutron in an (α,n) reaction within a thick material with macroscopic (α,n) cross section $\Sigma(E)$ and stopping power $dE/d\chi\ (E)$ is given by

$$P(E_\alpha) = \int_0^{E_\alpha} \frac{\Sigma(E)}{dE/d\chi\ (E)}\ dE \quad . \tag{14}$$

Values of $P(E_\alpha)$ for alpha particles in UF_6 were calculated using the POFEAL code, which employs the alogrithm

$$P(I) = (1.E + 6)* \sum_{i=2}^{I} \frac{N_F\ [\sigma_F(i-1) + \sigma_F(i)]/2}{N\ [\varepsilon(i-1) + \varepsilon(i)]/2}\ [E(i)-E(i-1)] \quad , \tag{15}$$

where

N_F is the atom density of ^{19}F(atoms/cm^3),
N is the total atom density (atoms/cm^3),
E(i) is the i-th regular energy point (MeV),
$\sigma_F(i)$ is the $^{19}F(\alpha,n)$ cross section at E(i) (mb), and
$\varepsilon(i)$ is the stopping cross secton at E(i) [eV/(10^{15} atoms/cm^2)].

The stopping cross section $\varepsilon(E)$ is related to the stopping power $dE/d\chi(E)$ by

$$\varepsilon(E) = \frac{1}{N}\ \frac{dE}{d\chi}(E) \quad , \tag{16}$$

and the value of the stopping cross section ε may be accumulated from the contributions from the J constituents using the Bragg-Kleeman relationship[46]

$$\varepsilon(E) \simeq \frac{1}{N} \sum_{j=1}^{J} N_j \varepsilon_j(E) \quad , \tag{17}$$

where

$$N = \sum_{j=1}^{J} N_j \quad . \tag{18}$$

Note that the factor 10^6 in Eq. (15) is required because of the units of σ_F, ε, and E.

Values of $\varepsilon(E)$ have been tabulated by Ziegler[47] for elements up to U(Z=92) over a wide energy range. Polynomial functions of the form

$$\ln[\varepsilon(E)] = C_0+C_1\ln(E)+C_2\ln^2(E)+C_3\ln^3(E)+C_4\ln^4(E) \tag{19}$$

have been fit to the data of Ziegler reflecting the tabulated values within $\pm$ 1% over the 0.5-10 MeV range of validity. The coefficients of the functions for F gas, F solid, and U solid are given in Table VIII.

The $^{19}F(\alpha,n)^{22}Na$ cross section given graphically by Balakrishnan et al.[48] over the energy range 2.55-4.97 MeV has been approximated by the 483-point linear-linear representation of Fig. 24, extending from the 2.36 MeV threshold[49] to the upper extent of the data. These functional expressions of $\varepsilon(E)$ and $\sigma_F(E)$ were used by the POFEAL code for the evaluation of $P(E_\alpha)$ using Eq. (15) at 4000 equally spaced energies over the range of the cross section. Calculated $P(E_\alpha)$ values differed by less than 5% when calculated alternately with fits to the F gas and F solid stopping cross section. The neutron production function $P(E_\alpha)$ calculated with the F gas stopping cross-section function is shown in Fig. 25. This function is extrapolated to 6 MeV with a dashed line to approximate neutron production at energies above the available cross-section data. An abbreviated table of $P(E_\alpha)$ values is given in Table IX.

The alpha-particle decay energies and intensities of U nuclides potentially present in UF_6 are combined with calculated $P(E_\alpha)$ values in Table X to determine the alpha spectrum-averaged neutron production probability for each U nuclide. These values are combined with the calculated spontaneous fission rates of Ref. 43 to determine total neutron production rates of each U nuclide. These total values are compared in Table XI with the measured and recommended values of Sampson.[50]

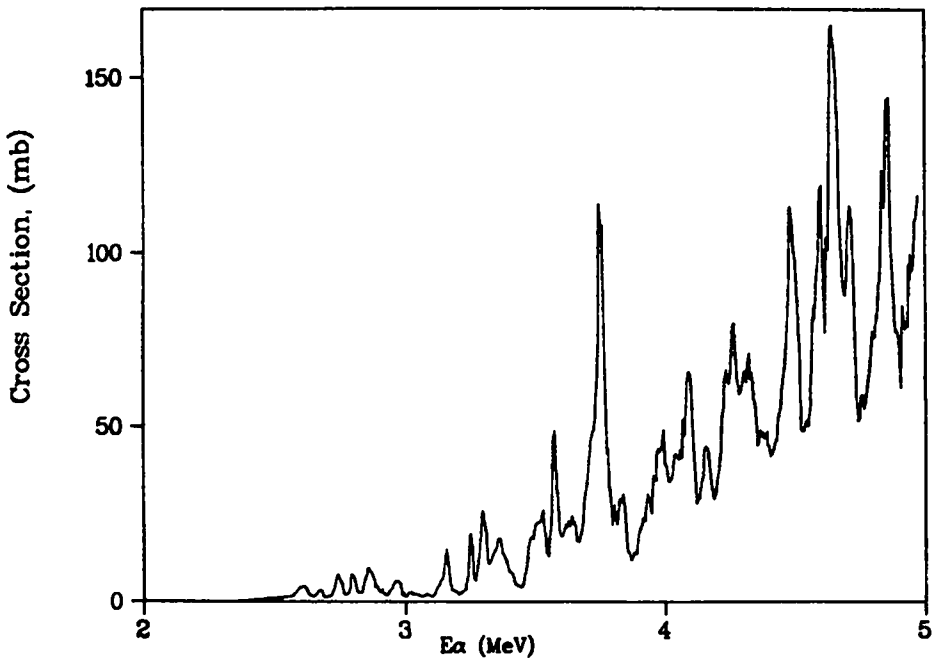

Fig. 24.
$^{19}F(\alpha,n)$ cross section from M. Balakrishnan, S. Kezilas, and M. K. Mehta (Ref.48).

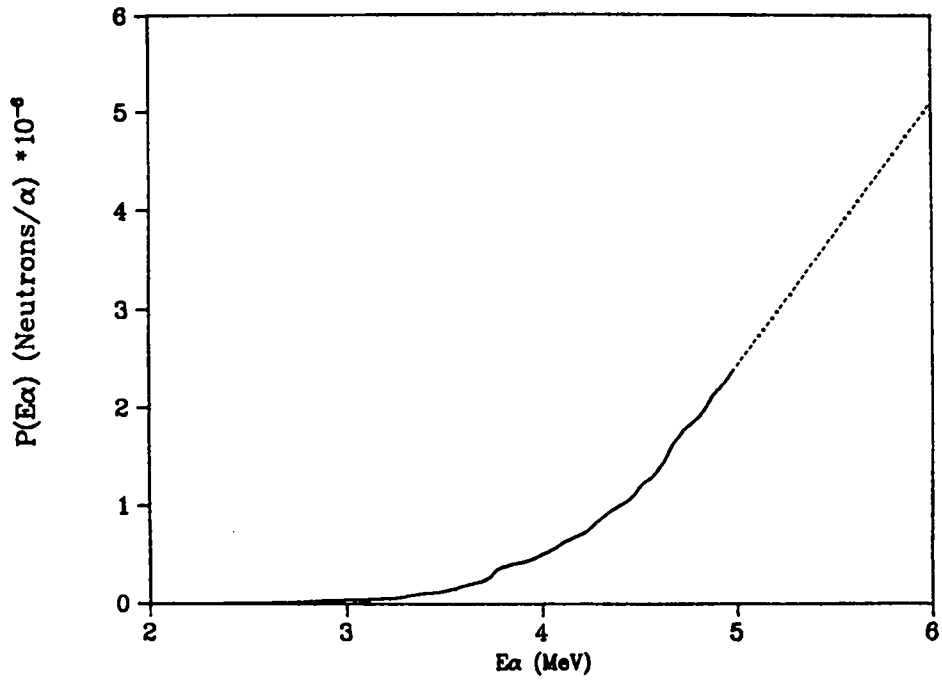

Fig. 25.
Neutron production function for decay α particles emitted at E_α in UF_6-thick target.

Thick target $P(E_\alpha)$ neutron production function values are not directly applicable to the production of neutrons in a gas centrifuge, where many alpha particles may escape the gas volume at alpha escape energies E'_α above the $^{19}F(\alpha,n)$ cross-section threshold. Neutron production probabilities

$$f(E_\alpha,E'_\alpha) = P(E_\alpha) - P(E'_\alpha) \quad , \tag{20}$$

for the 4.603-, 4.721-, and 4.773-MeV alpha-particle energies E_α of ^{234}U have been calculated at 3695 alpha-particle escape energies E'_α in the range $0. \leq E'_\alpha \leq 4.773$ MeV as shown in Fig. 26. An abbreviated table of these $f(E_\alpha,E'_\alpha)$ values is given in Table XII.

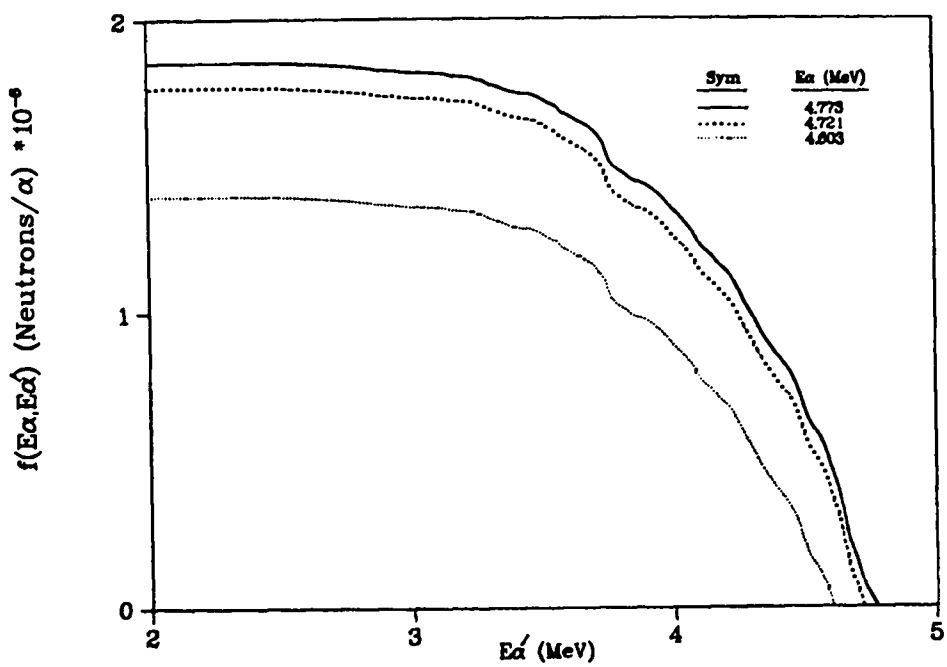

Fig. 26
Neutron production probability for the 4.603-, 4.721-, and 4.773-MeV alpha particles of ^{234}U prior to escape at energy E'_α.

TABLE VIII

FUNCTIONAL FITS TO STOPPING CROSS SECTIONS SX OF ZIEGLER
FOR ALPHAS IN THE ENERGY RANGE 0.5MEV<E<10.MEV
IN ELEMENTAL F(GAS), F(SOLID), AND U(SOLID)

```
ALOG(SX)=C0 + C1*(ALOG(E)) + C2*(ALOG(E)**2)
        + C3*(ALOG(E)**3) + C4*(ALOG(E)**4)
```

SX IN UNITS OF EV/(1E15 ATOMS/ CM**2)
E IN UNITS OF MEV

TERM	F(GAS)	F(SOLID)	U(SOLID)
C0	+3.82330+0	+3.70130+0	+5.16480+0
C1	-1.09172-1	-7.18301-2	-1.61478-1
C2	-3.02565-1	-3.04124-1	-2.79242-1
C3	+2.37259-2	+4.37674-2	+9.92320-2
C4	+1.08637-2	+3.69588-3	-1.46254-2

J.F.ZIEGLER,"HELIUM STOPPING POWERS AND RANGES
IN ALL ELEMENTAL MATTER," VOL 4 OF "THE STOPPING
AND RANGES OF IONS IN MATTER",PERGAMON PRESS(1977)

FUNCTIONAL FITS REFLECT DATA TO BETTER THAN 1%

TABLE IX

CALCULATED NEUTRON PRODUCTION FUNCTION VALUES
FOR ALPHA PARTICLES ON F-19 IN UF6--THICK TARGET

ALPHA PARTICLE ENERGY, MEV	NEUTRONS PER ALPHA PARTICLE*
2.36000E+00	0.
2.36065E+00	8.14636E-14
2.37242E+00	1.08527E-11
2.38810E+00	5.27509E-11
2.39986E+00	1.04944E-10
2.44757E+00	5.01087E-10
2.48416E+00	1.00833E-09
2.60376E+00	5.08146E-09
2.71550E+00	1.00071E-08
2.83052E+00	2.00058E-08
2.93051E+00	3.00159E-08
3.11283E+00	4.00326E-08
3.17687E+00	5.00365E-08
3.25399E+00	6.00173E-08
3.29189E+00	7.00045E-08
3.31346E+00	8.00386E-08
3.34940E+00	9.01890E-08
3.37750E+00	1.00168E-07
3.62910E+00	2.00221E-07
3.74346E+00	3.00532E-07
3.83822E+00	4.00303E-07
3.99440E+00	5.00575E-07
4.08785E+00	6.00577E-07
4.18719E+00	7.00432E-07
4.26038E+00	8.01307E-07
4.31985E+00	9.00600E-07
4.39435E+00	1.00047E-06
4.50413E+00	1.20031E-06
4.60281E+00	1.39438E-06
4.66293E+00	1.60073E-06
4.72110E+00	1.76402E-06
4.77338E+00	1.85181E-06
4.83807E+00	2.00003E-06
4.91061E+00	2.20018E-06
4.97335E+00	2.36505E-06

*THIRTY-FIVE VALUES ABOVE TAKEN
FROM 4000 VALUES CALCULATED.

TABLE X

CALCULATED (ALPHA,N) NEUTRON PRODUCTION BY U NUCLIDE DECAY ALPHAS ON F-19 IN UF6--THICK TARGET.

NUCLIDE	ALPHA ENERGY (MEV)	DECAY FRACTION	NEUTRONS PER 1E+6 ALPHAS	NEUTRONS PER 1E+6 DECAYS
U-230	5.662	.00230	4.196*	.00965
	5.666	.00360	4.207*	.01515
	5.818	.31903	4.611*	1.47105
	5.889	.67507	4.800*	3.24034
				*4.7
U-231	5.454	.000055	3.643*	* .00020
U-232	5.137	.00319	2.800*	.00893
	5.264	.31898	3.138*	1.00096
	5.320	.67783	3.287*	2.22803
				*3.2
U-233	4.729	.01616	1.782	.02880
	4.754	.00163	1.821	.00297
	4.783	.13246	1.868	.24744
	4.796	.00281	1.894	.00532
	4.825	.84694	1.960	1.66000
				1.94453
U-234	4.603	.00299	1.395	.00417
	4.721	.27916	1.764	.49244
	4.773	.71785	1.851	1.32874
				1.82535
U-235	4.155	.00899	.670	.00602
	4.218	.05697	.730	.04159
	4.274	.00400	.826	.00330
	4.327	.02998	.913	.02737
	4.329	.00210	.916	.00192
	4.363	.00350	.962	.00337
	4.367	.17989	.967	.17395
	4.382	.00300	.986	.00296
	4.398	.56966	1.005	.57251
	4.417	.03998	1.026	.04102
	4.440	.00700	1.056	.00739
	4.505	.01199	1.202	.01441
	4.558	.03698	1.282	.04741
	4.660	.04596	1.386	.06370
				1.00693
U-236	4.333	.00259	.922	.00239
	4.444	.25933	1.062	.27541
	4.492	.73808	1.170	.86355
				1.14135
U-238	4.041	.00100	.544	.00054
	4.150	.11488	.665	.07640
	4.199	.88412	.710	.62773
				0.70466

NEUTRON PRODUCTION VALUES FOR ALPHA ENERGIES ABOVE 4.973 MEV ARE EXTRAPOLATED FROM FIG.2 AS P[N/ALPHA]=-(1.08604-05) + E[MEV](2.65926-06)

TABLE X1

URANIUM NUCLIDE SPONTANEOUS FISSION NEUTRONS AND (ALPHA,N) NEUTRONS FROM ALPHAS ON F-19 IN UF6--THICK TARGET

	NEUTRONS PER NUCLIDE DECAY			NEUTRONS/S/KG OF NUCLIDE		
NUCLIDE	F-19 (ALPHA,N)	REF.44 SPON.FIS.	TOTAL	THIS WORK	REF.50 MEASURED	REF.50 RECOM'ND
U-230	4.7 -06	0.	4.7 -06	4.8 +12		
U-231	2.0 -10	0.	2.0 -10	1. +09		
U-232	3.2 -06	1.54 -12	3.2 -06	2.6 +09		
U-233	1.945-06	2.29 -12	1.945-06	6.940+05		
U-234	1.825-06	2.17 -11	1.825-06	4.220+05	5.76 +05 +/-2.0+4	5.76 +05 +/-4.2+4
U-235	1.007-06	3.74 -09	1.011-06	8.087+01	8.2 +01 +/-2.0+2	1.22 +02 +/-9.0+0
U-236	1.141-06	2.29 -09	1.144-06	2.738+03	2.86 +03 +/-1.2+4	3.95 +03 +/-2.9+2
U-238	7.047-07	1.095-06	1.800-06	2.240+01	2.787+01 +/-8.7-1	2.79 +01 +/-2.0+0

REF.44. W.B.WILSON,R.T.PERRY,T.R.ENGLAND,R.J.LABAUVE,M.E.BATTAT, AND N.L.WHITTEMORE,"NEUTRON PRODUCTION FROM ACTINIDE DECAY IN OXIDE FUELS", IN "APPLIED NUCLEAR DATA RESEARCH AND DEVELOPMENT, JULY 1 - SEPTEMBER 30, 1980",LOS ALAMOS SCIENTIFIC LABORATORY REPORT LA-8630-PR (DECEMBER,1980)

REF.50. T.E.SAMPSON,"NEUTRON YIELDS FROM URANIUM ISOTOPES IN URANIUM HEXAFLUORIDE,"NUCL.SCI.ENG.54,470(1974)

TABLE XII

NEUTRON PRODUCTION PROBABILITY F(E,E′) FOR THE E=4.603-,4.721-, AND 4.773-MEV U-234 ALPHA PARTICLES ON F-19 IN UF6 PRIOR TO ESCAPE AT ENERGY E′

E′, ALPHA ESCAPE ENERGY, MEV	UF6 NEUTRON PRODUCTION PROBABILITY*		
	E=4.603 MEV	E=4.721 MEV	E=4.773 MEV
0.	1.394380E-06	1.764020E-06	1.851810E-06
2.360000E+00	1.394380E-06	1.764020E-06	1.851810E-06
2.518150E+00	1.392740E-06	1.762380E-06	1.850170E-06
2.676290E+00	1.385582E-06	1.755222E-06	1.843012E-06
2.834440E+00	1.374090E-06	1.743730E-06	1.831520E-06
2.992590E+00	1.359090E-06	1.728730E-06	1.816520E-06
3.150730E+00	1.349344E-06	1.718984E-06	1.806774E-06
3.308880E+00	1.315942E-06	1.685582E-06	1.773372E-06
3.467030E+00	1.279330E-06	1.648970E-06	1.736760E-06
3.625180E+00	1.196131E-06	1.565771E-06	1.653561E-06
3.783320E+00	1.028770E-06	1.398410E-06	1.486200E-06
3.941470E+00	9.443960E-07	1.314036E-06	1.401826E-06
4.099620E+00	7.754090E-07	1.145049E-06	1.232839E-06
4.257760E+00	5.983160E-07	9.679560E-07	1.055746E-06
4.415910E+00	3.698400E-07	7.394800E-07	8.272700E-07
4.521780E+00	1.617700E-07	5.314100E-07	6.192000E-07
4.559030E+00	1.106700E-07	4.803100E-07	5.681000E-07
4.586470E+00	4.861000E-08	4.182500E-07	5.060400E-07
4.597580E+00	1.578000E-08	3.854200E-07	4.732100E-07
4.600850E+00	5.610000E-09	3.752500E-07	4.630400E-07
4.601500E+00	3.700000E-09	3.733400E-07	4.611300E-07
4.602160E+00	1.830000E-09	3.714700E-07	4.592600E-07
4.602810E+00	0.	3.696400E-07	4.574300E-07
4.629610E+00		3.001500E-07	3.879400E-07
4.656400E+00		1.891000E-07	2.768900E-07
4.706720E+00		4.278000E-08	1.305700E-07
4.717830E+00		9.240000E-09	9.703000E-08
4.719130E+00		5.460000E-09	9.325000E-08
4.719790E+00		3.610000E-09	9.140000E-08
4.720440E+00		1.790000E-09	8.958000E-08
4.721100E+00		0.	8.779000E-08
4.721750E+00			8.603000E-08
4.743970E+00			4.581000E-08
4.766190E+00			1.143000E-08
4.767490E+00			9.400000E-09
4.770110E+00			5.280000E-09
4.772070E+00			2.130000E-09
4.772720E+00			1.070000E-09
4.773380E+00			0.

*THIRTY-NINE VALUES ABOVE TAKEN FROM 3695 VALUES CALCULATED.

REFERENCES

1. D. C. Dodder and G. M. Hale, "Application of Approximate Isospin Conservation in R-Matrix Analysis," Proc. Int. Conf. on Neutron Physics and Nuclear Data, p. 490 (1978).

2. J. Frolich, L. Streit, H. Zankel, and H. Zingl, "Simple Coulomb Correction for Phase-Shifts and Applications to the p-p System," J. Phys. G6, 841 (1980).

3. J. Frolich, L. Steit, and H. Zankel, "Coulomb Corrections in N-N Coupled States," Phys. Lett 92B, 8 (1980).

4. M. I. Haftel and H. Zankel, "Approximate Coulomb Effects in the Three-Body Scattering Problem," submitted to Phys. Rev. C.

5. M. Gell-Mann and M. L. Goldberger, "The Formal Theory of Scattering," Phys. Rev. 91, 398 (1953).

6. P. A. Schmelzbach, W. Gruebler, R. E. White, V. Koenig, R. Risler, and P. Marmier, "Phase Shift Analysis of p-d Elastic Scattering," Nucl. Phys. A197, 273 (1972).

7. J. K. Dickens, T. A. Love, and G. L. Morgan, "Gamma-Ray Production Due to Neutron Interactions with Tungsten for Incident Neutron Energies between 1.0 and 20 MeV: Tabulated Differential Cross Sections," Oak Ridge National Laboratory report ORNL-4847 (1973).

8. G. L. Morgan, T. A. Love, J. K. Dickens, and F. G. Perey, "Gamma-Ray Production Cross Sections of Tantalum and Carbon for Incident Neutron Energies between 0.007 and 20 MeV," Oak Ridge National Laboratory report ORNL-TM-3702 (1972); also G. T. Chapman, G. L. Morgan, F. G. Perey, "A Re-Measurement of the Neutron-Induced Gamma-Ray Production Cross Sections for Iron in the Energy Range 850 keV $\leq E_n \leq$ 20.0 MeV," Oak Ridge National Laboratory report ORNL/TM-5416 (1976).

9. Darrell M. Drake, John C. Hopkins, C. S. Young, and H. Condé, "Gamma-Ray Production Cross Sections for Fast Neutron Interactions with Several Elements," Nucl. Sci. Eng. 40, 294 (1970).

10. M. B. Savin, Iu. A. Khoklov, I. N. Paramonova, V. A. Chirkin, V. N. Lunin, and N. N. Zalialov, "Total Gamma-Ray Production Cross Sections from the Interaction of 1-10 MeV Neutrons with Tungsten Nuclei," Proc. Fourth All Union Conf. on Neutron Physics, Kiev, Vol. 2, p. 103 (1978).

11. E. D. Arthur and C. A. Philis, "New Calculations of Neutron-Induced Cross Sections on Tungsten Isotopes," in "Applied Nuclear Data Research and Development July 1-September 30, 1980," Los Alamos Scientific Laboratory report LA-8630, p. 2 (1980).

12. A. B. Smith, Argonne National Laboratory, personal communication (1980).

13. R. C. Martin, P. F. Yergin, R. H. Augustson, N. N. Kaushal, H. A. Medicus, and E. J. Winhold, "MeV Neutron Total Cross Sections of Ta and W Isotopes," Bull. Am. Phys. Soc. 12, 106 (1967).

14. J. Frehaut, A. Bertin, R. Bois, and J. Jary, "Status of (n,2n) Cross Section Measurements at Bruyeres-le-Chatel," Proc. Symp. on Neutron Cross Sections from 10 to 50 MeV, May 1980, BNL-NCS-51245, Vol. 1, p. 399 (1980).

15. E. D. Arthur and D. G. Foster, Jr., "Average Neutronic Properties of 'Prompt' Fission Products," in "Applied Nuclear Data Research and Development, April 1-June 30, 1979," Los Alamos Scientific Laboratory report LA-8036-PR, p. 8 (1979).

16. P. G. Young and E. D. Arthur, "GNASH: A Preequilibrium, Statistical Nuclear-Model Code for Calculation of Cross Sections and Emission Spectra," Los Alamos Scientific Labortory report LA-6940 (1977).

17. C. L. Dunford, "Compound Nucleus Reaction Analysis Programs COMNUC and CASCADE," Atomics International report TI-707-130-013 (1971).

18. TCCAL consists primarily of spherical-optical-model routines excerpted from COMNUC.

19. O. Bersillon, "SCAT2 - A Spherical Optical Model Code," in "Progress Report of the Nuclear Physics Division, Bruyeres-le-Chatel, 1977," CEA-N-2037, p. 111 (1978).

20. C. Kalbach and F. M. Mann, "Phenomenology of Preequilibrium Angular Distributions," in Proc. Symp. on Neutron Cross Sections from 10 to 50 MeV, Brookhaven National Laboratory (1980) (to be published).

21. R. E. MacFarlane, Los Alamos Scientific Laboratory, personal communication to the Codes and Formats Subcommittee of the Cross Section Advisory Working Group (March, 1980).

22. D. G. Madland and J. R. Nix, "Calculation of Prompt Fission Neutron Spectra," Proc. of the Int. Conf. on Nuclear Cross Sections for Technology, Knoxville, TN, October 22-26, 1979, National Bureau of Standards Special Publication 594, p. 788 (1980).

23. D.G. Madland and J. R. Nix, "Calculation of Neutron Spectra and Average Neutron Multiplicities from Fission," in Proc. Int. Conf. on Nuclear Physics, Berkeley, CA, August 24-30, 1980 (to be published).

24. F. Manero and V. A. Konshin,"Status of the Energy-Dependent ν-Values for the Heavy Isotopes ($Z > 90$) from Thermal to 15 MeV and of ν-Values for Spontaneous Fission," At. Energ. Rev. 10, 637 (1972).

25. J. R. Smith, "Status of ^{252}Cf ν and Its Impact on Thermal Reactor Parameters," in Proc. of the Symp. on Nuclear Data Problems for Thermal Reaction Applications, May 22-24, Brookhaven National Laboratory, EPRI NP-1093 (ENDF-270) p. 5-1 (1979).

26. R. Kinsey, Ed., "Data Formats and Procedures for the Evaluated Nuclear Data File, ENDF," Brookhaven National Laboratory report ENDF-102, p. 5.4 (Oct. 1979).

27. R. J. LaBauve, D. C. George, D. W. Muir, P. D. Soran, and C. M. Eisenhauer, "Nuclear Data Development Work in Support of the Natioal Bureau of Standards ISNF Project February 1976-July 1980," Los Alamos Scientific Laboratory report LA-8638-MS (1980).

28. R. Douglas O'Dell, Forest W. Brinkley, Jr., and Duane R. Marr, "Users' Manual for ONEDANT: A Code Package for One-Dimensional, Diffusion-Accelerated, Neutral-Particle Transport," personal communication (1981).

29. R. E. MacFarlane, R. J. Barrett, D. W. Muir, and R. M. Boicourt, "The NJOY Nuclear Data Processing System: User's Manual," Los Alamos Scientific Laboratory report LA-7584-M (1978).

30. R. B. Kidman and R. E. MacFarlane, "LIB-V, A Library of Group Constants for Nuclear Reactor Calculations," personal communication (1981).

31. D. W. Muir, "Compact Representation of Neutron Activiation and Decay Data in Decay-Dominated Applications," p. 25 in "Applied Nuclear Data Research and Development Aprul 1-June 30, 1980," Los Alamos Scientific Laboratory report LA-8524-PR (1980).

32. T. R. England, W. B. Wilson, and M. G. Stamatelatos, "Fission Product Data for Thermal Reactors, Part 1: A Data Set for EPRI-CINDER Using ENDF/B-IV," Los Alamos Scientific Laboratory report LA-6745-MS (1976) and "Fission Product Data for Thermal Reactors, Part 2: User's Manual for EPRI-CINDER," Los Alamos Scientific Laboratory report LA-6746-MS (1976).

33. T. R. England, R. Wilczynski, and N. L. Whittemore, "CINDER-7: An Interim Users Report," Los Alamos Scientific Laboratory report LA-5885-MS (1975). [CINDER-10, the latest corresponding version in use, is described in "Applied Nuclear Data Research and Development October 1-December 31, 1975," p. 13, LA-6266-PR (1976), and "Applied Nuclear Data Research and Development January 1-March 31, 1976," p. 60, LA-6472-PR (1976).]

34. T. R. England, W. B. Wilson, and M. G. Stamatelatos, "Fission-Product Data for Thermal Reactors, Part 2: Users Manual for EPRI-CINDER Code and Data," Los Alamos Scientific Laboratory report LA-6746-MS (1976). [Also published as EPRI NP-356, Part 2 (1976).]

35. W. B. Wilson, T. R. England, and R. J. LaBauve, "Multigroup and Few-Group Cross Sections for ENDF/B-IV Fission Products; the TOAFEW Collapsing Code and Data File of 154-Group Fission-Product Cross Sections," Los Alamos Scientific Laboratory report LA-7174-MS (1978).

36. Fission Product Decay Library of the Evaluated Nuclear Data File, Versions IV and V (ENDF/B-IV and -V). (Available from and maintained by the National Nuclear Data Center at Brookhaven Natrional Laboratory.)

37. "American National Standards Institute/American Nuclear Society Standard, Decay Heat Power in Light Water Reactors," ANSI/ANS 5.1 (1979).

38. Personal communication, letter Tobias to England, dated Nov. 24, 1980.

39. Personal communication, letter Yoshida to England, dated Nov. 14, 1980.

40. T. Yoshida, Nucl. Sci. & Eng. 63, 376 (1977).

41. T. R. England, R. E. Schenter, and F. Schmittroth, "Integral Decay-Heat Measurements and Comparisons to ENDF/B-IV and -V," Los Alamos Scientific Laboratory report LA-7422-MS (1978).

42. H. Henryson, Argonne National Laboratory, personal communication, letter to T. R. England, dated 12-10-80.

43. R. T. Perry and W. B. Wilson, "The (α,n) Neutron Production by Alpha Particles in PuO_2,UO_2, and ThO_2 Fuels," in "Applied Nuclear Data Research and Development April 1 - June 30, 1980, " Los Alamos Scientific Laboratory report LA-8524-PR, p. 20 (1980).

44. W. B. Wilson, R. T. Perry, T. R. England, R. J. LaBauve, M. E. Battat, and N. L. Whittemore, "Neutron Production from Actinide Decay in Oxide Fuels," in "Applied Nuclear Data Research and Development, July 1 - September 30, 1980," Los Alamos Scientific Laboratory report LA-8630-PR, p. 23 (1980)

45. R. T. Perry and W. B. Wilson, "Neutron Production from (α,n) Reactions in PuO_2, UO_2, and ThO_2 Fuels," Trans. Am. Nucl. Soc. 35, 549 (1980).

46. W. H. Bragg and R. Kleeman, "On the Alpha Particles of Radium and Their Loss of Range in Passing Through Various Atoms and Molecules," Phil. Mag. 10, 318 (1905).

47. J. F. Ziegler, Helium Stopping Powers and Ranges in All Elemental Matter," Vol. 4 of The Stopping and Ranges of Ions in Matter (Pergamon Press, New York, 1977).

48. M. Balakrishnan, S. Kailas, and M. K. Mehta, "A Study of the Reaction $^{19}F(\alpha,n)^{22}Na$ in the Bombarding Energy Range 2.6 to 5.1 MeV," Pramana 10, 329 (1978).

49. L. Van der Zwan and K. W. Geiger, "Energy Levels in ^{23}Na from the $^{19}F(\alpha,n)^{22}Na$ Reaction," Nucl. Phys. A284, 189 (1977).

50. T. E. Sampson, "Neutron Yields from Uranium Isotopes in Uranium Herafluoride," Nucl. Sci. Eng. 54, 470 (1974).

☆U.S. GOVERNMENT PRINTING OFFICE: 1981-0-777-022/35

Printed in the United States of America
Available from
National Technical Information Service
US Department of Commerce
5285 Port Royal Road
Springfield, VA 22161

Microfiche $3.50 (A01)

Page Range	Domestic Price	NTIS Price Code	Page Range	Domestic Price	NTIS Price Code	Page Range	Domestic Price	NTIS Price Code	Page Range	Domestic Price	NTIS Price Code
001-025	$ 5.00	A02	151-175	$11.00	A08	301-325	$17.00	A14	451-475	$23.00	A20
026-050	6.00	A03	176-200	12.00	A09	326-350	18.00	A15	476-500	24.00	A21
051-075	7.00	A04	201-225	13.00	A10	351-375	19.00	A16	501-525	25.00	A22
076-100	8.00	A05	226-250	14.00	A11	376-400	20.00	A17	526-550	26.00	A23
101-125	9.00	A06	251-275	15.00	A12	401-425	21.00	A18	551-575	27.00	A24
126-150	10.00	A07	276-300	16.00	A13	426-450	22.00	A19	576-600	28.00	A25
									601-up	†	A99

†Add $1.00 for each additional 25-page increment or portion thereof from 601 pages up.